Supporting Information

Nano-Assemblies from J-Aggregated Dyes: A Stimuli-Responsive Tool Applicable to Living Systems

Meihui Su[1,2], Shuoxin Li[1,2], Hao Zhang[1], Junqing Zhang[1,2], Haoliang Chen[1,2], and Changhua Li[1,2,3]*

E-mail: chli@nankai.edu.cn (C.L.)

[1]State Key Laboratory of Medicinal Chemical Biology, Nankai University, Tianjin 300071, P. R. China. [2]College of Pharmacy, Nankai University, Tianjin 300071, P. R. China. [3]Key Laboratory of Functional Polymer Materials of Ministry of Education, Nankai University, Tianjin 300071, P. R. China.

Table of Contents

1. Materials and Instruments

Unless otherwise noted, reagents were used as received from commercial sources. Solvent preparations were carried according to described procedures.[1] Trypsin-EDTA (0.25%), and 3-(4,5-dimethylthiazol-2-yl)-2,5-diphenyltetrazolium bromide (MTT) were purchased from Invitrogen. Dulbecco's Modified Essential Medium (DMEM), fetal bovine serum (FBS), and 10 × phosphate buffer saline (PBS; pH 7.4) were purchased from Gibco (Life Technologies, AG, Switzerland). Lipopolysaccharide (LPS), 3-morpholinosydnonimine (SIN-1), 2′,7′-dichlorfluorescein-diacetate (DCF-DA), 1,3-diphenylisobenzofuran (DPBF), methylene blue (MB), interferon-γ (IFN-γ), minocycline hydrochloride, poly(ethylene glycol) methyl ether (PEG-OH; average M_n 5,000), *ε*-caprolactone (*ε*-CL), and Tin(II) 2-ethylhexanoate ($Sn(Oct)_2$) were purchased from Sigma-Aldrich. Water was deionized with a Milli-Q SP reagent water system (Millipore) to a specific resistivity of 18.2 MΩcm. Compound **1**,[2] **3a**,[3] **3b**,[4] **5**,[2] and 4-(3-phenyltzobenzofuryl)phenyl trimethylammonium iodide (QDPBF),[5] were synthesized according to literature procedures.

^1H and ^{13}C NMR spectra were recorded at 25 °C on a Bruker AV400 NMR spectrometer, operating at 400 and 100 MHz, respectively, where chemical shifts (δ in ppm) were determined using partially or non-deuterated solvent residues as internal references. DMSO-d_6 and $CDCl_3$ were used as the solvents. High-resolution mass spectra (HRMS) were obtained on Varian 7.0T FTMS. HPLC analysis was performed with a Shimadzu HPLC system, equipped with a LC-20AT binary pump, an SPD-20A UV-vis detector, and a Symmetry C18 column. Dynamic light scattering (DLS) studies were performed using a Zetasizer NanoZS (Malvern). Morphological analyses were conducted on cryogenic transmission electron microscopy transmission (cryo-TEM; Talos F200C), transmission electron microscopy (TEM; Talos F200C, FEI), and atomic force microscopy (AFM; Dimension Icon, Bruker). UV-Vis absorbance spectra were recorded on a UH5300 double-beam UV-Vis spectrophotometer (Hitachi). MTT assay was monitored by the microplate reader (SpectraMax i3x, MD). Cells fluorescence images were obtained by an inverted fluorescence microscope (ZOE Fluorescent Cell Imager, BIO-RAD). Confocal laser scanning microscopy (CLSM) images were acquired using a Leica TCS SP8 microscope. Cell flow experiments were detected with flow cytometry (BD LSRFortessa, BD).

2. Chemical synthesis

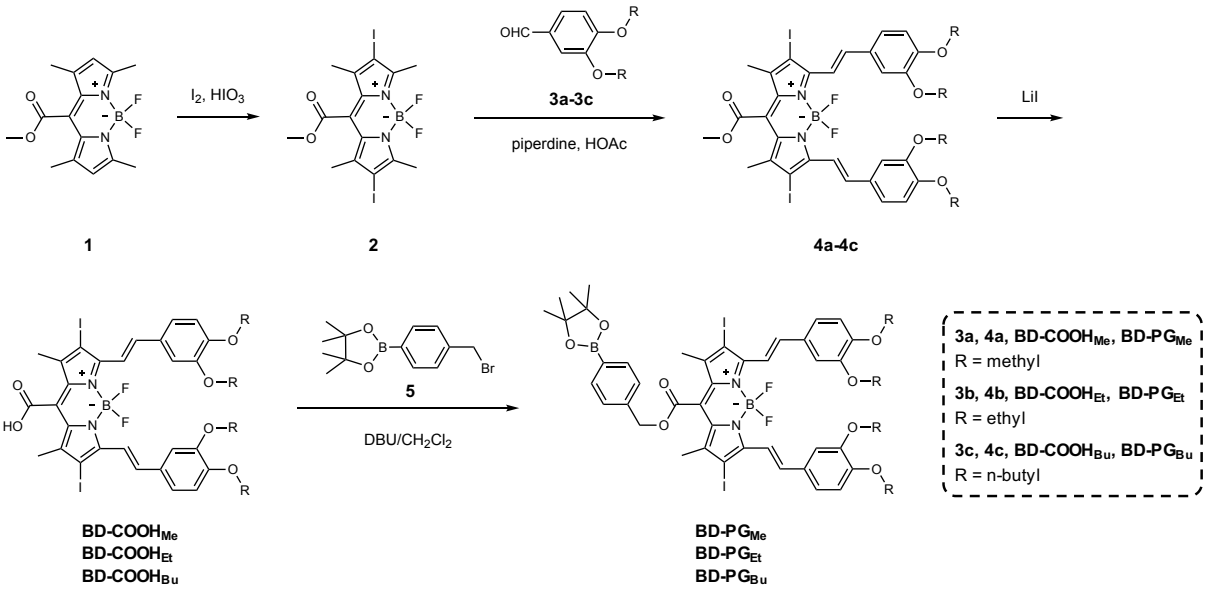

Scheme 1. Synthetic routes employed for the preparation of **BD-PG$_R$** (**BD-PG$_{Me}$**, **BD-PG$_{Et}$**, and **BD-PG$_{Bu}$**).

2.1 Synthesis of compound 2

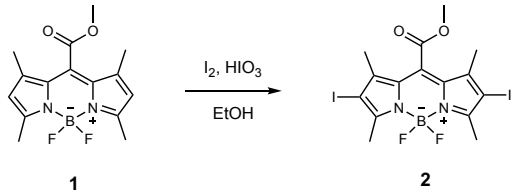

2: To a stirred solution of compound **1** (1.2 g, 4.0 mmol) and I_2 (2.54 g, 10.0 mmol) in ethanol (100 mL) was added a solution of HIO_3 (1.4 g, 8.0 mmol) in water (2.0 mL), and the resulting mixture was stirred at 60 °C for about 40 min and monitored by TLC. After the reaction was completed, saturated sodium thiosulfate solution was added (100 mL) and stirred at room temperature for additional 30 min. Then, the mixture was extracted with dichloromethane (CH_2Cl_2; 3 × 200 mL). The combined organic layer was washed with saturated brine, dried over sodium sulfate and evaporated under reduced pressure, affording compound **2** as a golden solid (2.0 g, yield: 90.5%). ^{1}H NMR (400 MHz, $CDCl_3$, Figure S31) δ (ppm) 4.00 (s, 3H), 2.62 (s, 6H), 2.13 (s, 6H).

2.2 Synthesis of compound 3c

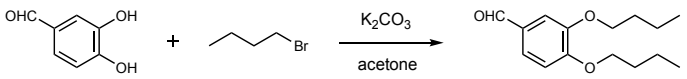

3c

3c: To a stirred suspension of 3,4-dihydroxybenzaldehyde (1.38 g, 10.0 mmol), K_2CO_3 (6.9 g, 50.0 mmol) and KI (0.30 g) in dry acetone (100 mL), a solution of bromobutane (2.68 mL, 25.0 mmol) in dry acetone (5 mL) was added dropwise, and the resulting mixture was stirred at reflux overnight. After filtration and removing the solvent, the residue was dissolved in EtOAc, and washed twice with saturated brine, dried over sodium sulfate, and evaporated to dryness. The residue was chromatographed on silica gel with petroleum ether (PE)/EtOAc (50/1, v/v) as an eluent, affording **3c** as white solid (2.28 g, yield: 91.2%). ^{1}H NMR (400 MHz, $CDCl_3$, Figure S32) δ (ppm) 9.83 (s, 1H), 7.46–7.37 (m, 2H), 6.96 (d, J = 8.0 Hz, 1H), 4.08 (m, 4H), 1.84 (m, 4H), 1.52 (m, 4H), 0.99 (m, 6H).

2.3 Synthesis of compound 4a-4c

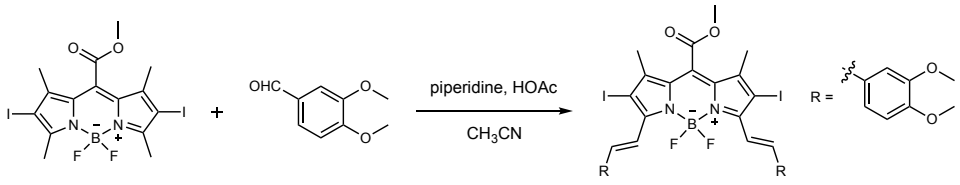

2 **3a** **4a**

4a: To a solution of **3a** (498.5 mg, 3.0 mmol) in dry acetonitrile (CH_3CN, 30 mL) was added piperidine (0.5 mL) and acetic acid (HOAc, 0.5 mL), and the mixture was stirred for 10 min at room temperature before the addition of **2** (557.9 mg, 1.0 mmol). The resulting mixture was stirred for additional 5 h at room temperature, under argon and dry molecular sieves which were used to remove the produced water. The mixture was dissolved in EtOAc and washed twice with saturated ammonium chloride (NH_4Cl) solution and saturated brine, dried over sodium sulfate. After filtration and removing the solvent, the residue was chromatographed on silica gel with PE/CH_2Cl_2 (1/5, v/v) as eluent, affording **4a** as a dark red metallic solid (0.56 g, yield: 65.5%). ^{1}H NMR (400 MHz, $CDCl_3$, Figure S33) δ (ppm) 8.16 (d, J = 16.6 Hz, 2H), 7.53 (d, J = 16.6 Hz, 2H), 7.22 (d, J = 8.4 Hz, 2H), 7.15 (s, 2H), 6.90 (d, J = 8.4 Hz, 2H), 4.02 (s, 3H), 3.95 (d, J = 9.6 Hz, 12H), 2.21 (s, 6H).

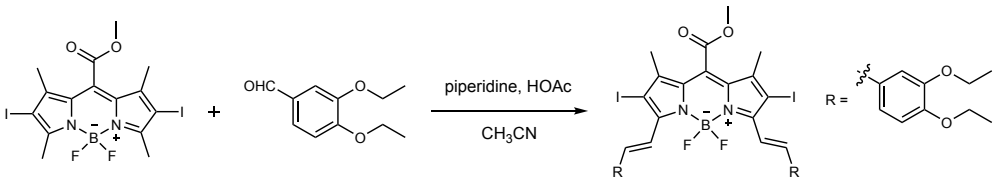

2 3b 4b

4b: **4b** was synthesized according to the same procedure as that used for **4a**. **4b**, a dark red metallic solid, yield: 69.3%. ^{1}H NMR (400 MHz, $CDCl_3$, Figure S34) δ (ppm) 8.14 (d, J = 16.5 Hz, 2H), 7.51 (d, J = 16.5 Hz, 2H), 7.21 (d, J = 8.4 Hz, 2H), 7.15 (d, J = 2.1 Hz, 2H), 6.89 (d, J = 8.4 Hz, 2H), 4.16 (m, 8H), 4.01 (s, 3H), 2.20 (s, 6H), 1.49 (t, J = 6.9 Hz, 12H).

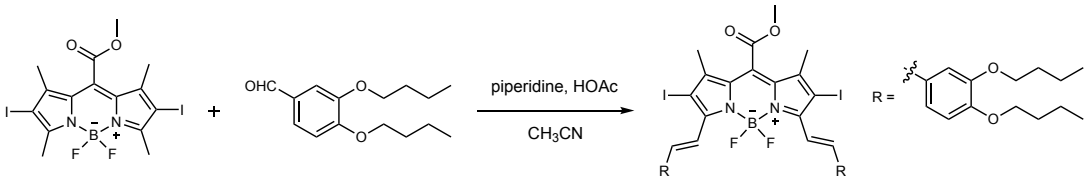

2 3c 4c

4c: **4c** was synthesized according to the same procedure as that used for **4a**. **4c**, a dark red metallic solid, yield: 65.2%. ^{1}H NMR (400 MHz, $CDCl_3$, Figure S35) δ (ppm) 8.15 (d, J = 16.5 Hz, 2H), 7.51 (d, J = 16.5 Hz, 2H), 7.22 (d, J = 8.4 Hz, 2H), 7.14 (s, 2H), 6.89 (d, J = 8.4 Hz, 2H), 4.06 (m, 8H), 3.99 (s, 3H), 2.19 (s, 6H), 1.83 (m, 8H), 1.52 (m, 8H), 0.99 (m,12H).

2.4 Synthesis of BD-COOH$_{Me}$, BD-COOH$_{Et}$, and BD-COOH$_{Bu}$

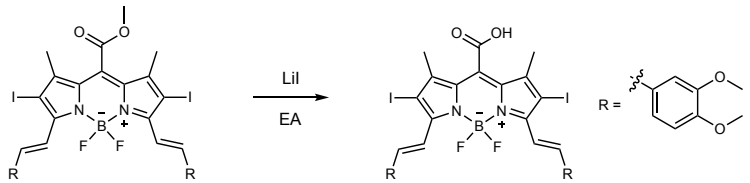

4a BD-COOH$_{Me}$

BD-COOH$_{Me}$: To a solution of **4a** (0.43 g, 0.5 mmol) in dry EtOAc (50 mL) was added lithium iodide (0.27 g, 2.0 mmol), and the mixture was stirred at reflux for about 4 h under an argon atmosphere. After cooling to room temperature, EtOAc (100 mL) was added to the resulting mixture. The mixture was washed with 0.1 N HCl and saturated brine, dried over sodium sulfate. After filtration and removing the solvent, the residue was chromatographed on silica gel with CH_2Cl_2/methanol (100/3 v/v) as an eluent, affording **BD-COOH$_{Me}$** as a dark red metallic solid (0.26 g, yield: 61.9%). ^{1}H NMR (400

MHz, DMSO-d_6, Figure S36) δ (ppm) 8.07 (d, J = 16.6 Hz, 2H), 7.40 (d, J = 16.6 Hz, 2H), 7.21 (d, J = 8.4 Hz, 2H), 7.18 (s, 2H), 7.07 (d, J = 8.4 Hz, 2H), 3.83 (d, J = 6.8 Hz, 12H), 2.31 (s, 6H). ^{13}C NMR (100 MHz, DMSO-d_6, Figure S37) δ (ppm) 166.10, 150.65, 150.18, 149.14, 143.81, 139.21, 129.12, 128.87, 121.18, 116.24, 112.09, 109.90, 83.74, 55.70, 55.46, 15.34. HRMS (ESI, Figure S51): m/z $[M-H]^+$ calcd for $C_{32}H_{28}BF_2I_2N_2O_6$ 839.0103; found 839.0100.

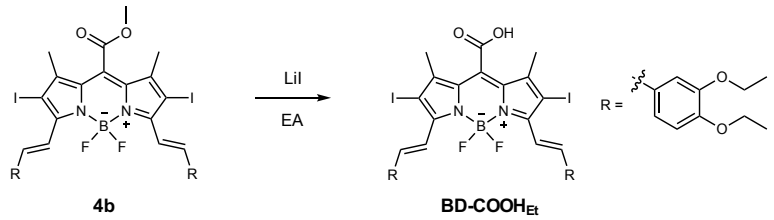

4b **BD-COOH$_{Et}$**

BD-COOH$_{Et}$: **BD-COOH$_{Et}$** was synthesized according to the same procedure as that used for **BD-COOH$_{Me}$**. **BD-COOH$_{Et}$**, a dark red metallic solid, yield: 62.4%. ^{1}H NMR (400 MHz, DMSO-d_6, Figure S38) δ (ppm) 7.94 (d, J = 16.6 Hz, 2H), 7.37 (d, J = 16.6 Hz, 2H), 7.20–7.10 (m, 4H), 7.04 (d, J = 8.7 Hz, 2H), 4.09 (m, 8H), 2.37 (s, 6H), 1.36 (t, J = 6.1 Hz, 12H). ^{13}C NMR (100 MHz, DMSO-d_6, Figure S39) δ (ppm) 165.03, 149.67, 148.45, 148.02, 144.13, 140.10, 137.31, 129.19, 129.08, 120.65, 116.64, 113.31, 111.39, 81.57, 63.91, 63.88, 15.51, 14.82, 14.75. HRMS (ESI, Figure S52): m/z $[M-H]^+$ calcd for $C_{36}H_{36}BF_2I_2N_2O_6$ 895.0729; found 895.0733.

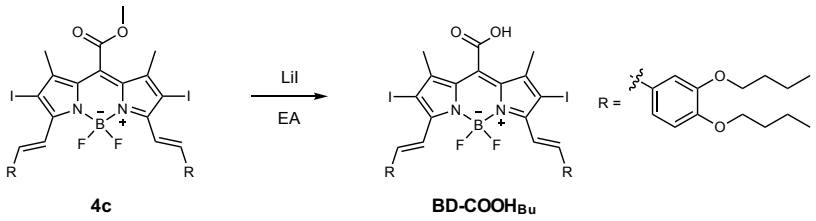

4c **BD-COOH$_{Bu}$**

BD-COOH$_{Bu}$: **BD-COOH$_{Bu}$** was synthesized according to the same procedure as that used for **BD-COOH$_{Me}$**. **BD-COOH$_{Bu}$**, a dark red metallic solid, yield: 66.1%. ^{1}H NMR (400 MHz, DMSO-d_6, Figure S40) δ (ppm) 8.06 (d, J = 16.5 Hz, 2H), 7.38 (d, J = 16.5 Hz, 2H), 7.17 (m, 4H), 7.02 (d, J = 8.0 Hz, 2H), 4.02 (m, 8H), 2.30 (s, 6H), 1.71 (m, 8H), 1.45 (m, 8H), 0.93 (m, 12H). ^{13}C NMR (100 MHz, DMSO-d_6, Figure S41) δ (ppm) 164.84, 150.01, 148.79, 147.85, 144.05, 140.56, 137.15, 129.21, 129.16, 120.61, 116.67, 113.69, 111.93, 81.38, 68.21, 68.08, 30.92, 30.81, 18.80, 15.47, 13.76. HRMS (ESI, Figure S53): m/z $[M-H]^+$ calcd for $C_{44}H_{52}BF_2I_2N_2O_6$ 1007.1981; found 1007.1985.

2.5 Synthesis of BD-PG$_{Me}$, BD-PG$_{Et}$, and BD-PG$_{Bu}$

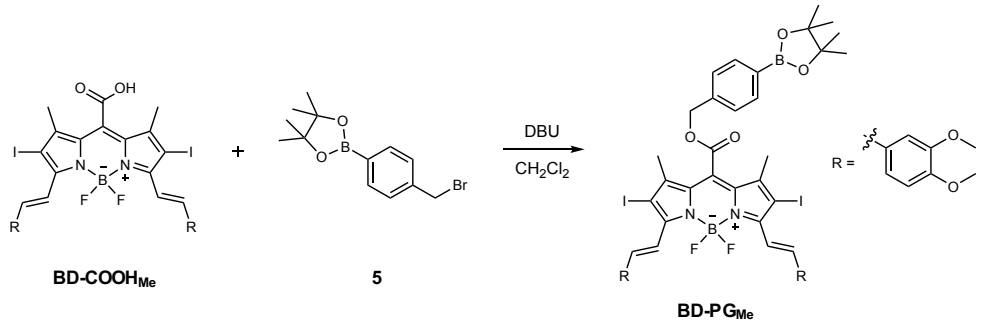

BD-COOH$_{Me}$ **5** **BD-PG$_{Me}$**

BD-PG$_{Me}$: To a solution of **BD-COOH$_{Me}$** (84 mg, 0.1 mmol), 1,8-diazabicyclo[5.4.0] undec-7-ene (DBU; 22 μL, 0.15 mmol) in dry CH_2Cl_2 (10 mL), **PG-Br** (89 mg, 0.3 mmol) was added, and the resulting mixture was stirred under an argon atmosphere at room temperature overnight. After removing the solvent, the residue was chromatographed on silica gel with CH_2Cl_2/methanol (100/0.5 v/v) as an eluent, affording **BD-PG$_{Me}$** as a green solid (59 mg, yield: 55.9%). ^{1}H NMR (400 MHz, $CDCl_3$, Figure S42) δ (ppm) 8.15 (d, J = 16.5 Hz, 2H), 7.85 (d, J = 7.5 Hz, 2H), 7.52 (d, J = 16.5 Hz, 2H), 7.45 (d, J = 7.5 Hz, 2H), 7.21 (d, J = 8.4 Hz, 2H), 7.14 (s, 2H), 6.88 (d, J = 8.4 Hz, 2H), 5.44 (s, 2H), 3.94 (d, J = 9.5 Hz, 12H), 2.13 (s, 6H), 1.36 (s, 12H). ^{13}C NMR (100 MHz, $CDCl_3$, Figure S43) δ (ppm) 165.26, 151.71, 150.84, 149.29, 143.72, 140.31, 136.17, 135.40, 130.44, 129.81, 128.37, 125.17, 122.23, 116.90, 111.21, 109.80, 84.16, 82.96, 68.85, 56.08, 56.04, 25.00, 15.82. HRMS (MALDI, Figure S54): m/z $[M]^+$ calcd for $C_{45}H_{46}B_2F_2I_2N_2O_8$ 1056.1498; found 1056.1503.

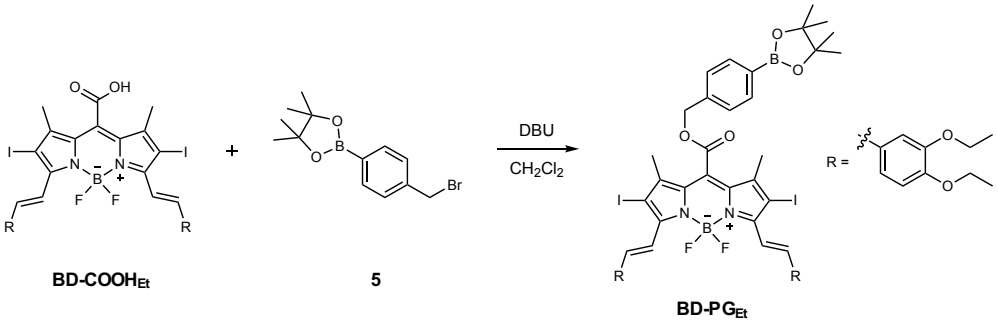

BD-COOH$_{Et}$ **5** **BD-PG$_{Et}$**

BD-PG$_{Et}$: **BD-PG$_{Et}$** was synthesized according to the same procedure as that used for **BD-PG$_{Me}$**. **BD-PG$_{Et}$**, a green solid, yield: 56.3%. ^{1}H NMR (400 MHz, $CDCl_3$, Figure S44) δ (ppm) 8.13 (d, J = 16.5 Hz, 2H), 7.85 (d, J = 7.5 Hz, 2H), 7.50 (d, J = 16.5 Hz, 2H), 7.44 (d, J = 7.5 Hz, 2H), 7.20 (d, J = 8.4 Hz, 2H), 7.15 (s, 2H), 6.89 (d, J = 8.4 Hz, 2H), 5.43 (s, 2H), 4.16 (m, 8H), 2.12 (s, 6H), 1.48 (t, J = 7.0 Hz, 12H), 1.36 (s, 12H). ^{13}C NMR (100 MHz, $CDCl_3$, Figure S45) δ (ppm) 165.34, 151.77, 150.69, 148.95,

143.62, 140.46, 136.21, 135.41, 130.46, 129.77, 128.36, 125.04, 122.18, 116.79, 112.99, 112.29, 84.17, 82.99, 68.85, 64.84, 64.65, 25.02, 15.83, 14.98, 14.88. HRMS (MALDI, Figure S55): m/z $[M]^+$ calcd for $C_{49}H_{54}B_2F_2I_2N_2O_8$ 1112.2124; found 1112.2131.

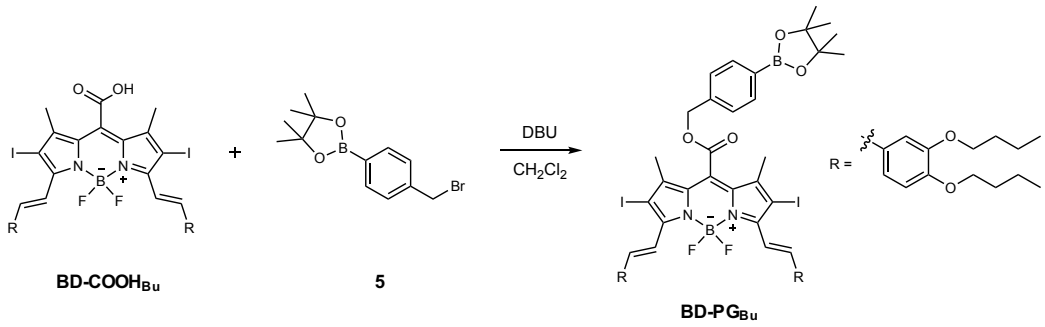

BD-COOH$_{Bu}$ **5** **BD-PG$_{Bu}$**

BD-PG$_{Bu}$: **BD-PG$_{Bu}$** was synthesized according to the same procedure as that used for **BD-PG$_{Me}$**. **BD-PG$_{Bu}$**, a green solid, yield: 53.3%. ^{1}H NMR (400 MHz, $CDCl_3$, Figure S46) δ (ppm) 8.13 (d, J = 16.5 Hz, 2H), 7.85 (d, J = 8.4 Hz, 2H), 7.57–7.39 (m, 4H), 7.21 (d, J = 8.4 Hz, 2H), 7.13 (s, 2H), 6.89 (d, J = 8.4 Hz, 2H), 5.44 (s, 2H), 4.06 (m, 8H), 2.12 (s, 6H), 1.83 (m, 8H), 1.60–1.45 (m, 8H), 1.36 (s, 12H), 0.98 (m, 12H). ^{13}C NMR (100 MHz, $CDCl_3$, Figure S47) δ (ppm) 165.31, 151.75, 151.12, 149.31, 143.55, 140.54, 136.20, 135.38, 130.42, 129.75, 128.34, 124.96, 122.00, 116.71, 113.34, 112.90, 84.13, 83.01, 69.20, 68.93, 68.80, 31.45, 31.31, 24.99, 19.38, 19.33, 15.80, 14.06, 14.00. HRMS (MALDI, Figure S56): m/z $[M]^+$ calcd for $C_{57}H_{70}B_2F_2I_2N_2O_8$ 1224.3376; found 1224.3383.

2.6 Synthesis of the amphiphilic diblock copolymer P$_n$ (n = 8, 50, and 80)

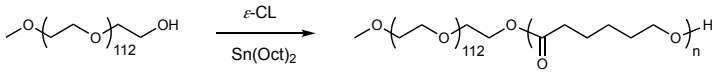

PEG-OH **PEG-PCL$_n$ (P$_n$)**

Amphiphilic diblock poly(ethylene glycol)-block-polycaprolactone (**P$_n$**) copolymers were synthesized through ring-opening polymerization of ε-CL using PEG-OH as a macroinitiator and $Sn(Oct)_2$ as the catalyst.[6] Take the synthesis of **P$_8$** as a typical example, ε-CL (1.08 g, 9.46 mmol), PEG-OH (5.0 g, 1.0 mmol), and $Sn(Oct)_2$ (1.1 mg, 2.7 μmol) were added into a fresh flamed and nitrogen purged round-bottomed flask. The mixture was stirred at 130 °C for 5 h. After cooling to room temperature, the resulting polymers were dissolved in dichloromethane and precipitated in an excess of cold ether. The precipitate was dried at room temperature under vacuum to afford **P$_8$** as a white solid. (5.8 g, yield: 95.4%). The degree of polymerization (DP; n) of PCL

segments were determined by ^{1}H NMR spectra (400 MHz, $CDCl_3$, Figures S48, S49, and S50 for **P_8**, **P_{50}**, and **P_{80}**, respectively).

3. Preparation and characterization of BD-PG_R/P_n nano-assemblies

3.1 Self-assembly of BD-PG_R/P_n

Typically, **P_n** (**P_8**, **P_{50}**, and **P_{80}**; 4 mg) and **BD-PG_R** (**BD-PG_{Me}**, **BD-PG_{Et}**, and **BD-PG_{Bu}**; 0-0.16 μmol) were dissolved in 0.5 mL acetone, followed by the addition of 10 mL deionized water under vigorous stirring at 900 rpm over 10 min at 37 °C. The resulting solution was stirred overnight under this condition, led to most of the acetone be evaporated. Residual acetone was removed under reduced vacuum. After passing through a 0.45 μm filter, the final solutions of nano-assemblies (conc. 0.4 g/L **P_n**; 0-13.6 μM **BD-PG_R**) were kept at room temperature.

3.2 Estimation of the fraction of J-aggregated dyes (α_J)

The fraction of J-aggregated dyes (α_J) was estimated according to a previous report.[7] The absorbance at 788 nm (A_{788}) is considered as the sum of the absorbance of J-aggregate and monomer. Thus, the fraction of J-aggregated dyes (α_J) can be calculated according to the following equations (1) and (2):

$$A_{788} = \varepsilon_{J788} c \alpha_J + \varepsilon_{m788} c \alpha_m \quad \text{..... (1)}$$

$$\alpha_J + \alpha_m = 1 \quad \text{..... (2)}$$

where c is the concentration of BODIPY dyes, α_m is the fraction of monomers, and ε_{m788} and ε_{J788} are the absorption coefficients of the monomeric and fully J-aggregated BODIPYs at 788 nm, respectively. ε_{J788} was estimated based on the assumption that BODIPY dyes completely formed J-aggregates (α_J = 1) within **BD-PG_{Me}/P_8** at a dye content of 2.0% (Figure S4a). On the other hand, **BD-PG_{Me}** dyes were demonstrated to remain in the monomeric state (α_m = 1) within **BD-PG_{Me}/P_{80}** at a dye content of 0.4% (Figure S3). Therefore, this sample was utilized to determine ε_{m788} (Figure S4b).

3.3 DLS sizing and morphological analysis

Dynamic light scattering (DLS). For particle size and polydispersity index (PDI) measurement, the stock solutions were 4-fold diluted with deionized water and passed through a 0.45 *μm* filter. Measurements were made in triplicate at 25 °C using Zetasizer

NanoZS. Zetasizer Nano software (version 7.12) was used to analyze the data.

Cryogenic transmission electron microscopy (cryo-TEM).[8] Cyro-TEM observations were performed on a Talos F200C electron microscope at an acceleration voltage of 200 kV. Typically, 5 *μ*L aqueous solution were dropped to perforated (1 *μ*m hole diameter) carbon film covered 200 mesh copper grids (R2/1 batch of Quantifoil Micro Tools GmbH, Jena, Germany). The grid was held by tweezers mounted on a Vitrobot Mark IV equipped with a controlled humidity (100%) and temperature (24 °C) environment. The sample was blotted and plunged into a liquid ethane reservoir cooled by liquid nitrogen. The vitrified samples were transferred to a Gatan 626 cryo-holder through a cryo-transfer stage cooled by liquid nitrogen. During observation of the vitrified samples, the cryo-holder temperature was maintained below -180°C.

Transmission electron microscopy (TEM). Typically, 5 *μ*L of diluted aqueous solutions (conc. 0.1 g/L $\mathbf{P_n}$) of nano-assemblies were dropped to a 200-mesh carbon coated copper grid and air-dried for 3 days. TEM observations were conducted on a Talos F200C electron microscope at an acceleration voltage of 200 kV.

Atomic force microscopy (AFM). AFM images were acquired with a Nanoscope V system operating in peakforce tapping mode under ambient condition. SNL-A cantilevers with a resonance frequency of ca. 65 kHz were used. The samples were prepared by dip coating 50 *μ*L of diluted aqueous solutions (conc. 0.1 g/L $\mathbf{P_n}$) of nano-assemblies onto freshly cleaved mica surfaces.

3.4 Stability studies

Stability of ***BD-PG$_{Me}$/P$_8$*** *nano-assemblies upon diluting*. Five diluted solutions of **BD-PG$_{Me}$/P$_8$** nano-assemblies were obtained through five 2-fold diluting with PBS starting from the stock solution of **BD-PG$_{Me}$/P$_8$** (conc. 0.4 g/L **P$_8$**; 8.0 *μ*M **BD-PG$_{Me}$**) at 25 °C.

Stability of ***BD-PG$_{Me}$/P$_8$*** *nano-assemblies in saline.* Saline solutions (containing 28.0% NaCl, w/v) with different volume were added to the stock solution of **BD-PG$_{Me}$/P$_8$** to produce a serial of saline solutions of **BD-PG$_{Me}$/P$_8$** (conc. 0.25 g/L **P$_8$**; 5.0 *μ*M **BD-PG$_{Me}$**) with different NaCl concentrations from 0 to 9.0% (w/v).

Stability of ***BD-PG$_{Me}$/P$_8$*** *nano-assemblies in cell culture medium.* The stock solution of **BD-PG$_{Me}$/P$_8$** was added to the RAW 264.7 cell culture medium (DMEM supplemented with 10% heat-inactivated FBS, 100 U/mL penicillin, and 100 *μ*g/mL streptomycin) at 25 °C to give a final solution of **BD-PG$_{Me}$/P$_8$** suspended in cell culture medium (conc. 0.1 g/L **P$_8$**; 2.0 *μ*M **BD-PG$_{Me}$**).

3.5 Peroxynitrite-triggered **BD-PG$_{Me}$/P$_8$** to **BD-COO$^-_{Me}$/P$_8$** conversion

*Peroxynitrite-induced **BD-PG$_{Me}$** to **BD-COO$^-_{Me}$** conversion.* Peroxynitrite ($OONO^-$, 0-4.0 μM) was added to the solution of **BD-PG$_{Me}$** (4.0 μM) in the mixture of CH_3CN/H_2O (10/1, v/v), and incubated for 1 min at 37 °C. UV-visible absorption spectrophotometer and HPLC were adopted to monitor peroxynitrite-induced **BD-PG$_{Me}$** to **BD-COO$^-_{Me}$** conversion. HPLC was performed by using an isocratic elution program with a solvent system of acetonitrile (0.5% TFA) at a flow rate of 1.0 mL/min with detection wavelength at 650 nm.

*Peroxynitrite-triggered **BD-PG$_{Me}$/P$_8$** to **BD-COO$^-_{Me}$/P$_8$** conversion.* Peroxynitrite ($OONO^-$, 10.0 μM) was added to the aqueous solution of **BD-PG$_{Me}$/P$_8$** (conc. 0.1 g/L **P$_8$**; 2.0 μM **BD-PG$_{Me}$**) in PBS (10 mM, pH 7.4), and incubated for 10 min at 37 °C. UV-visible absorption spectra of the mixture were recorded every 1 min to evaluate the time-dependent **BD-PG$_{Me}$/P$_8$** to **BD-COO$^-_{Me}$/P$_8$** conversion triggered by peroxynitrite. DLS, TEM, and AFM were utilized to study the size and shape of the converted **BD-COO$^-_{Me}$/P$_8$** aggregates.

Specificity of the peroxynitrite-triggered conversion. The specificity of peroxynitrite-triggered **BD-PG$_{Me}$/P$_8$** to **BD-COO$^-_{Me}$/P$_8$** conversion towards other ROSs (including H_2O_2, *t*BuOO•, OH•, and ClO^-) and some representative nucleophiles (including H_2S, HSO_3^-, SO_3^{2-}, SO_4^{2-}, Cys, and GSH) was investigated by UV-visible absorption spectrophotometer. According to the same process of peroxynitrite incubation as described above, representative ROSs and nucleophiles (5 equiv for ClO^- and $OONO^-$; 100 equiv for other species) were added to the solution of **BD-PG$_{Me}$/P$_8$** (conc. 0.1 g/L **P$_8$**; 2.0 μM **BD-PG$_{Me}$**) in PBS (10 mM, pH 7.4). Data were collected after 10 min incubation at 37 °C in PBS.

4. Detection of $^1O_2$ production in solution

Detection of singlet oxygen ($^1O_2$) production using QDPBF as probe.[5] Typically, 10 μM $OONO^-$ was added to the aqueous solution of **BD-PG$_R$/P$_n$** (conc. 0.05 g/L **P$_n$**; 1.0 μM **BD-PG$_R$**), and the mixture incubated at 37 °C for about 30 min. After the $OONO^-$-induced conversion from **BD-PG$_R$/P$_n$** to **BD-COO^-_R/P$_n$** was completed determined by UV-visible spectra, water soluble QDPBF was added to the solution, and the resulting mixture was then placed in a cuvette and subjected to light irradiation (655 nm, 5 mW/cm^2) for 90 seconds. The change in absorbance of QDPBF (ΔAbs) at 412 nm was

recorded at 10 s intervals to evaluate the photosensitivity in producing $^1O_2$. ΔAbs = Abs_0 – Abs; where Abs_0 and Abs are the absorbance of QDPBF at 412 nm before and after light irradiation, respectively.

Determination of singlet oxygen quantum yield (Φ_Δ). According to reported methods,[9,10] Φ_Δ of **BD-PG$_{Me}$/P$_8$** or **BD-COO$^-_{Me}$/P$_8$** was measured using methylene blue (MB) as a reference with $^1O_2$ quantum yield ($\Phi_{\Delta,MB}$) of 0.39 in PBS.[11] In these experiments, QDPBF was added to the sample solution, and subjected to the light irradiation (655 nm, 2 mW/cm^2) for 180 seconds. ΔAbs of QDPBF at 412 nm was recorded at 10 s intervals to obtain the decay rate of the photosensitizing process. The singlet oxygen quantum yield was calculated by using the following formula:

$$\boldsymbol{\Phi}_{\Delta,\text{sample}} = \boldsymbol{\Phi}_{\Delta,\text{MB}} \frac{\boldsymbol{K}_{\text{sample}} \boldsymbol{A}_{\text{MB}}}{\boldsymbol{K}_{\text{MB}} \boldsymbol{A}_{\text{sample}}},$$

where K_{sample} and K_{MB} are the decomposition rate constants of QDPBF by the samples and MB, respectively. A_{sample} and A_{MB} represent the light absorbed by the samples and MB, respectively, which are determined by the absorbances of the samples and MB at 655 nm, respectively. According to the same method, $^1O_2$ quantum yields of **BD-PG$_{Me}$** and **BD-COOH$_{Me}$** in DMSO/water (8/2, v/v) were determined by using MB as a reference with $^1O_2$ quantum yield ($\Phi_{\Delta,MB}$) of 0.52 in DMSO[12].

5. Biological studies

5.1 Cell culture and acquisition of activated RAW 264.7 cells

Cell culture. RAW 264.7 cell line was purchased from American Type Culture Collection (ATCC). The cells were cultured in DMEM supplemented with 10% heat-inactivated FBS, penicillin (100 U/mL), and streptomycin (100 μg/mL) in a 37 °C incubator with 5% CO_2. Before experiment, the cells were pre-cultured until confluence was reached to about 75%.

Acquisition of activated RAW 264.7 cells. After cultured for ca. 24 h, RAW 264.7 cells were treated with LPS (1 μg/mL) and INF-γ (50 ng/mL) for about 20 h to get the activated RAW 264.7 cells according to previous report.[13]

5.2 Intracellular $^1O_2$ Production

To assess the effectiveness of intracellular $OONO^-$ in activating our caged nano-

photosensitizers (**^{nano}PS-PG**) after internalization, dichlorofluorescein diacetate (DCF-DA) was chosen as an oxidant-sensitive fluorescent dye to detect the formed $^1O_2$, which rapidly oxidized DCF-DA into highly fluorescent dichlorofluorescein (DCF).[14,15] Typically, RAW 264.7 cells were incubated with **^{nano}PS-PG** (containing 1.0 μM **BD-PR$_{Me}$**) for 30 min, the medium was replaced with fresh DMEM containing SIN-1 at varying concentrations. Following treating with SIN-1 for 2 h, the cells were washed twice with PBS, freshly prepared DCF-DA solution (10 μM) in PBS was added and the cells were incubated for another 20 min. The cells were then washed with PBS, and subjected to red LED light irradiation (620-660 nm, 15 mW/cm^2) for 5 min and imaged on an inverted fluorescence microscope (ZOE Fluorescent Cell Imager, BIO-RAD).

5.3 Cell viability assay

Live/Dead staining and flow cytometric analysis. Normal RAW 264.7 or activated RAW 264.7 (upon incubation with LPS/IFN-γ for 20 h) macrophages were incubated with **^{nano}PS-PG** (containing 1.0 μM **BD-PG$_{Me}$**). After incubation for 2 h, the cells were washed twice with PBS, and subjected to red LED light irradiation (620-660 nm, 15 mW/cm^2) for 5 min. After photoirradiation, cells were incubated for 4 h, and stained with Calcein AM (1.0 μM) and Propidium Iodide (PI; 6.0 μM). After staining for 20 min, the cells were washed with PBS and imaged immediately by CLSM (Leica TCS SP8 microscope) or analyzed using flow cytometry (BD LSRFortessa, BD).

MTT assay. The RAW 264.7 cells were seeded in 96-well plates at an initial density of ca. 1 × 10^4 cells per well. After cultured for 24 h, the cells were activated with LPS (1.0 μg/mL) and INF-γ (50 ng/mL) for 20 h to obtain the activated RAW 264.7 cells. It should be noted that for control normal RAW 264.7 cell line, cells were incubated for 20 h in the absence of LPS and INF-γ. The medium was replaced with fresh DMEM containing **^{nano}PS-PG** at varying concentrations (containing 0, 0.5, 1.0, or 2.0 μM **BD-PG$_{Me}$**). After incubation for 2 h, the cells were washed with PBS and subjected to red LED light irradiation (620-660 nm, 15 mW/cm^2) over different time period (0, 1, 3, or 5 min). After 12 h incubation, freshly prepared MTT solution (150 μL, 0.5 mg/mL) in culture medium was added into each well. The cells were further incubated for 4 h at 37 °C. The MTT medium in each well was then carefully removed and replaced by DMSO (150 μL). The plate was gently agitated to dissolve all the precipitates formed. The absorbance at 570 nm was monitored by the microplate reader (SpectraMax i3x, MD). Cell viability was expressed by the ratio of absorbance of the cells incubated with **^{nano}PS-PG** to that of the cells incubated with culture medium only.

6. Supplementary figures

6.1 Characterization of BD-PG$_R$/P$_n$ nano-assemblies

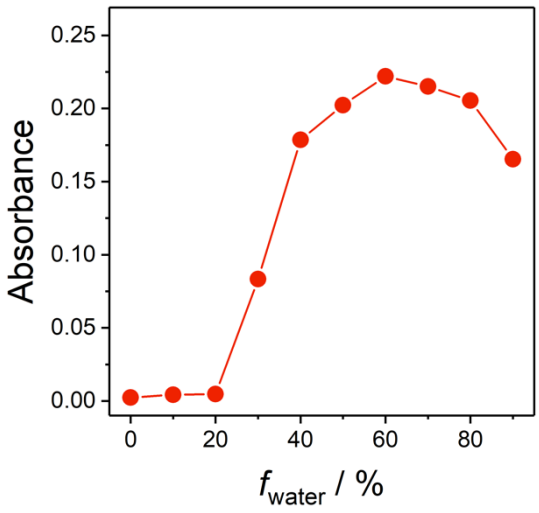

Figure S1. Changes in absorbance at respective $\lambda_{J\text{-}agg}$ of **BD-PG$_{Me}$** (4.0 μM) nano-assemblies in DMSO/water mixture with different water fraction (f_{water}, 0–90%) at 25 °C.

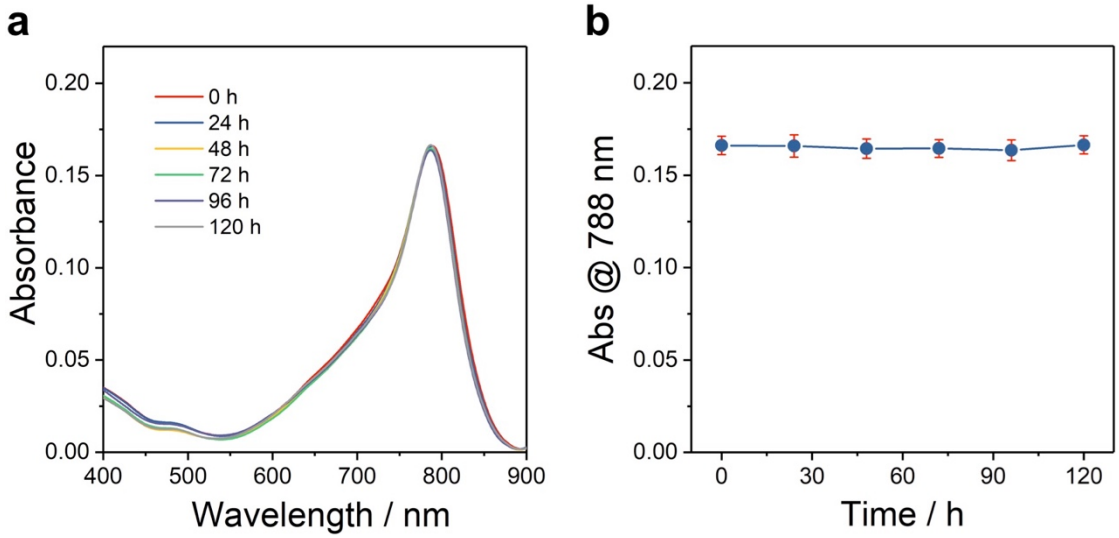

Figure S2. Time-dependent (a) UV-visible absorption spectra and (b) changes in absorbance at 788 nm (Abs @ 788 nm) recorded for **BD-PG$_{Me}$** (4.0 μM) in the DMSO/water mixture with 90% water content at 25 °C. Spectra were recorded every 24 hours over a period of five days.

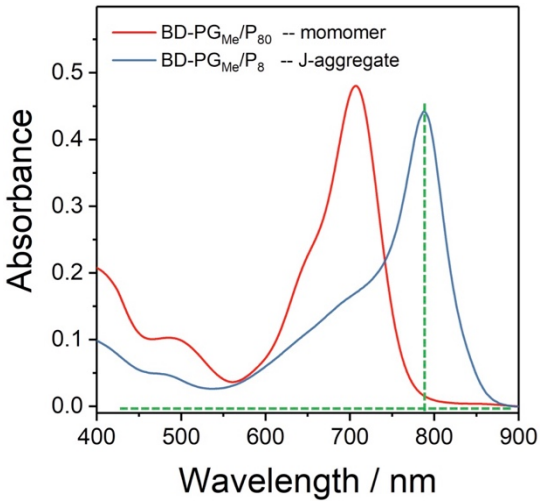

Figure S3. UV-visible absorption spectra recorded for aqueous solutions of **BD-PG$_{Me}$/P$_8$** (conc. 8.0 μM **BD-PG$_{Me}$**; 0.4 g/L **P$_8$**) and **BD-PG$_{Me}$/P$_{80}$** (conc. 8.0 μM **BD-PG$_{Me}$**; 2.0 g/L **P$_{80}$**) at 25 °C.

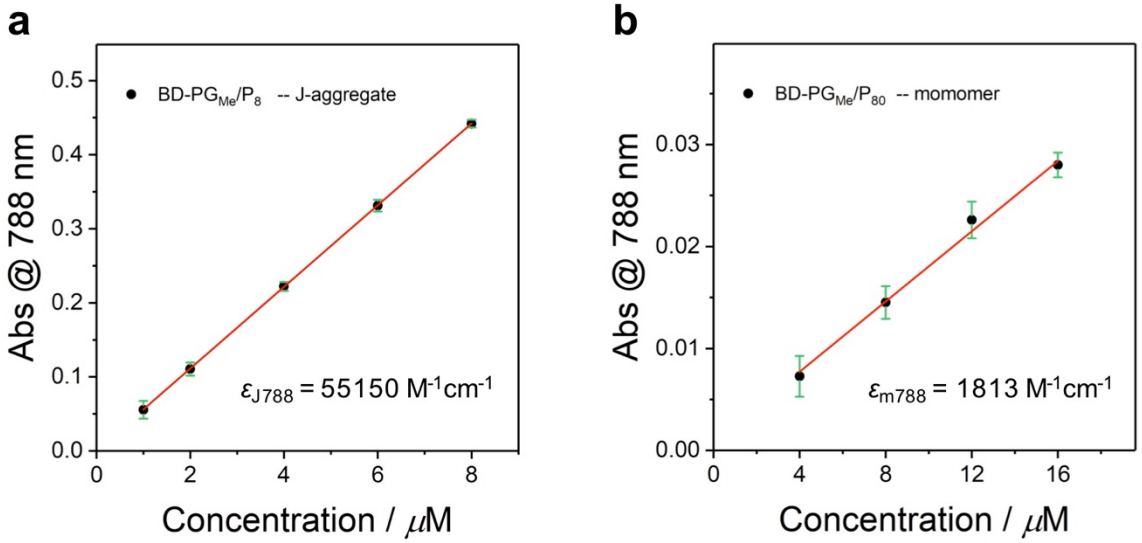

Figure S4. UV-visible calibration curves of (a) **BD-PG$_{Me}$/P$_8$** and (b) **BD-PG$_{Me}$/P$_{80}$** in water at 25 °C.

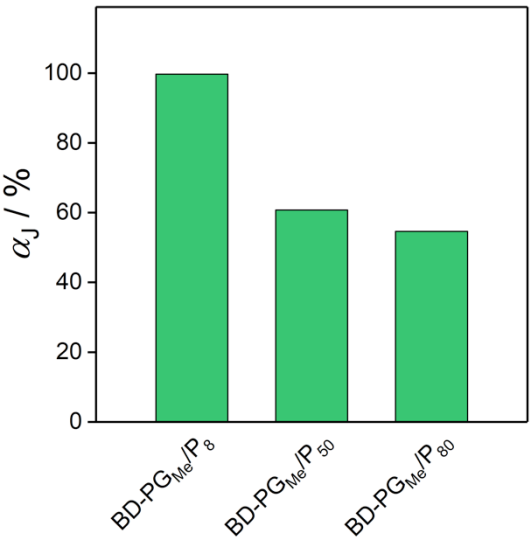

Figure S5. The fractions of J-aggregated BODIPY dyes (α_J) recorded for **BD-PG$_{Me}$/P$_8$**, **BD-PG$_{Me}$/P$_{50}$**, and **BD-PG$_{Me}$/P$_{80}$** at 25 °C. Conc. 0.2 g/L **P$_n$**, 4.0 μM **BD-PG$_{Me}$**.

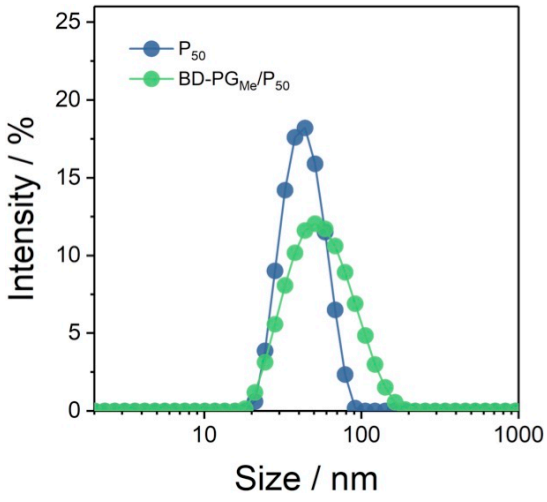

Figure S6. Size distribution of the micelles of **P$_{50}$** (steel blue) and **BD-PG$_{Me}$/P$_{50}$** (green) using dynamic light scattering (DLS) at 25 °C.

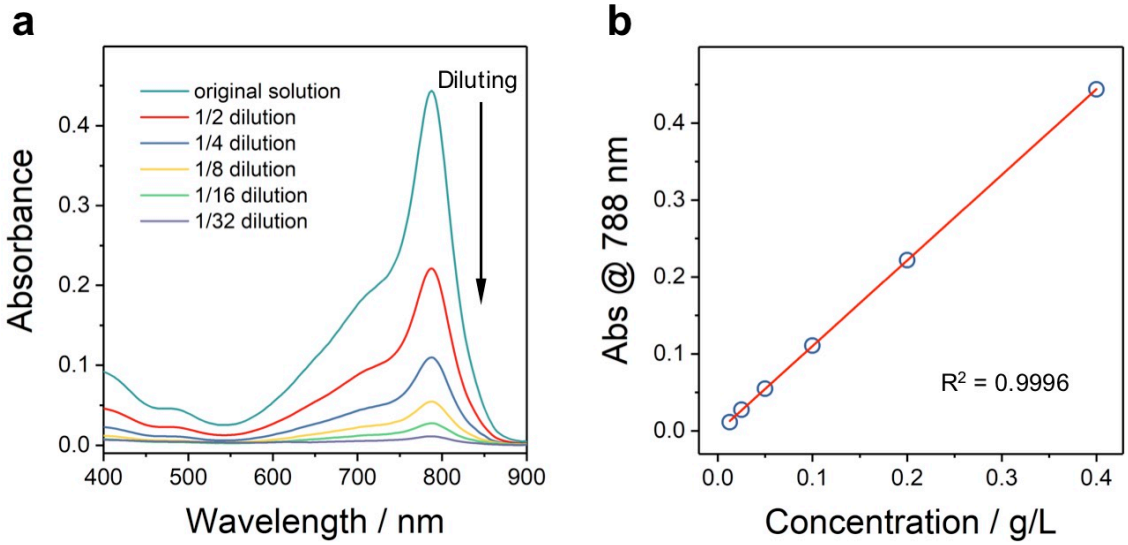

Figure S7. (a) UV-visible absorption spectra and (b) concentration-dependent changes of absorbance at 788 nm (Abs @ 788 nm) recorded for **BD-PG$_{Me}$/P$_8$** following five 2-fold serial dilutions with PBS at 25 °C. The concentrations of **BD-PG$_{Me}$** and **P$_8$** in the original solution were 8.0 μM and 0.4 g/L, respectively.

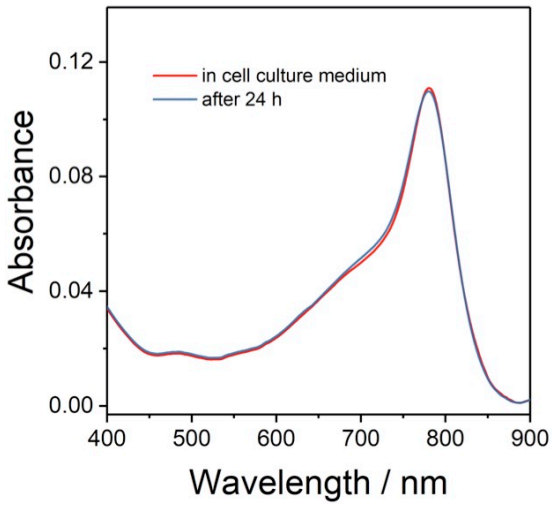

Figure S8. UV-visible absorption spectra recorded for **BD-PG$_{Me}$/P$_8$** (conc. 2.0 μM **BD-PG$_{Me}$**; 0.1 g/L **P$_8$**) in serum-containing cell culture medium (10% FBS) over a 24 h time period.

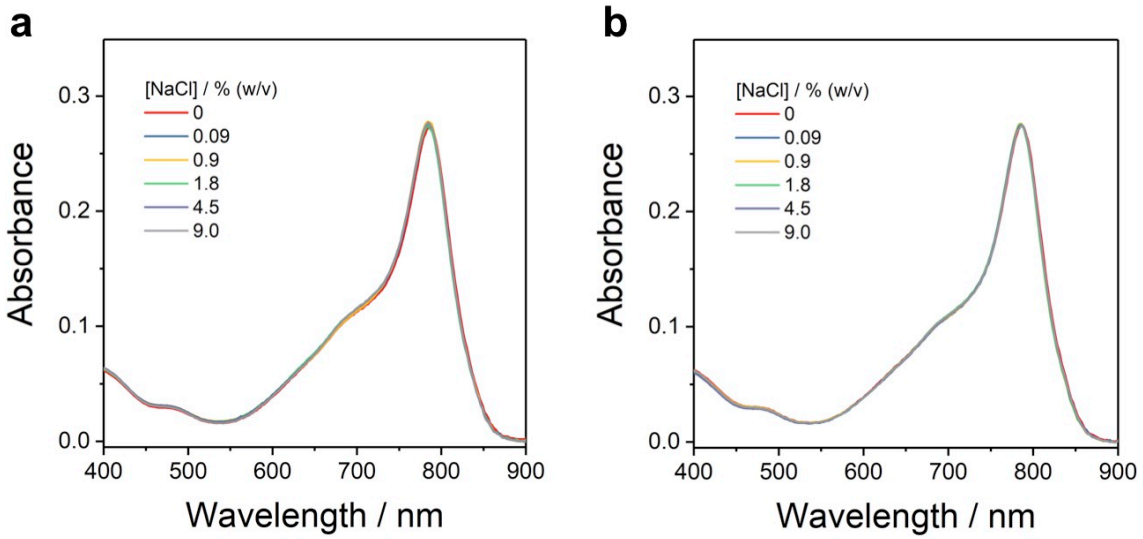

Figure S9. UV-visible absorption spectra recorded for **BD-PG$_{Me}$/P$_8$** (conc. 5.0 μM **BD-PG$_{Me}$**; 0.25 g/L **P$_8$**) in saline solution with different concentrations of sodium chloride (NaCl) from 0-9.0% (w/v) at 25 °C. Spectra recorded (a) immediately or (b) 24 hours after addition of NaCl.

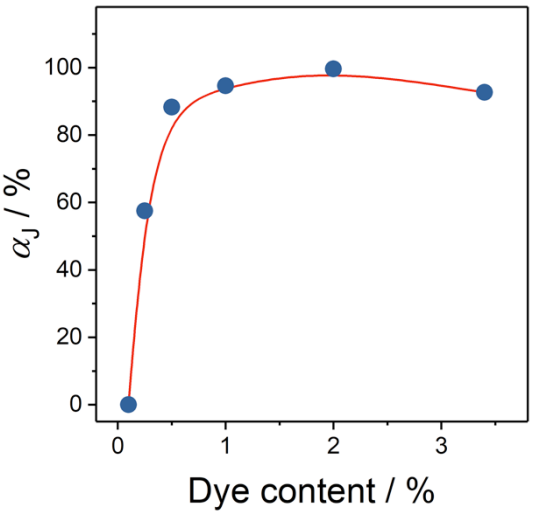

Figure S10. The fractions of J-aggregated BODIPY dyes (α_J) recorded for **BD-PG$_{Me}$/P$_8$** with different **BD-PG$_{Me}$** contents (0.1–3.4%) at 25 °C. The concentration of **P$_8$** was fixed at 0.4 g/L.

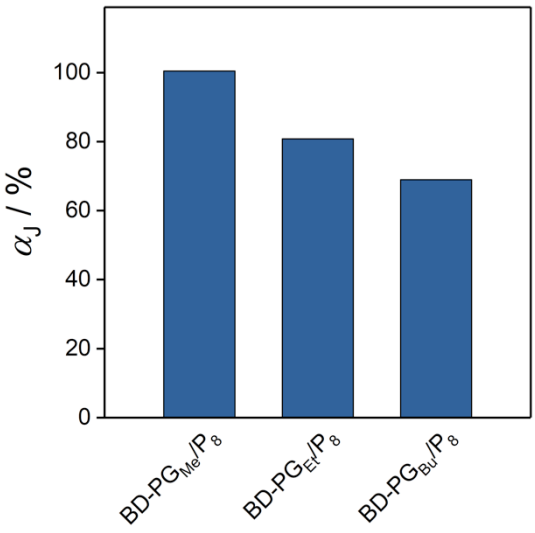

Figure S11. The fractions of J-aggregated BODIPY dyes (α_J) recorded for **BD-PG$_{Me}$/P$_8$**, **BD-PG$_{Et}$/P$_8$**, and **BD-PG$_{Bu}$/P$_8$** at 25 °C. Conc. 0.2 g/L **P$_8$**, 4.0 μM **BD-PG$_R$**.

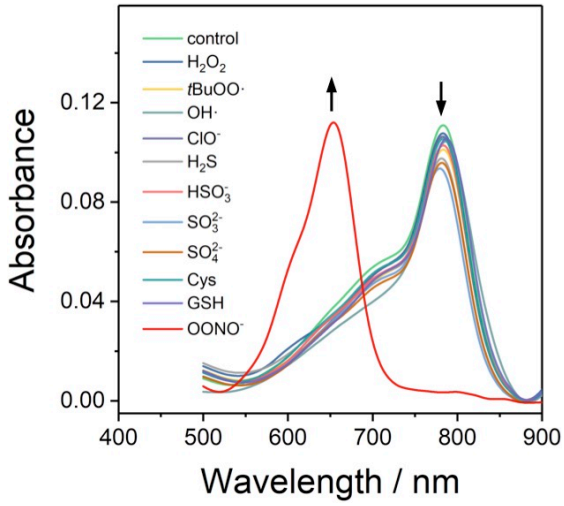

Figure S12. UV−visible absorption spectra recorded for **BD-PG$_{Me}$/P$_8$** (conc. 2.0 μM **BD-PG$_{Me}$**; 0.1 g/L **P$_8$**) upon incubation with various ROSs and some typical physiological nucleophiles (5 equiv for ClO^- and $OONO^-$; 100 equiv for other species) for 10 min at 37 °C.

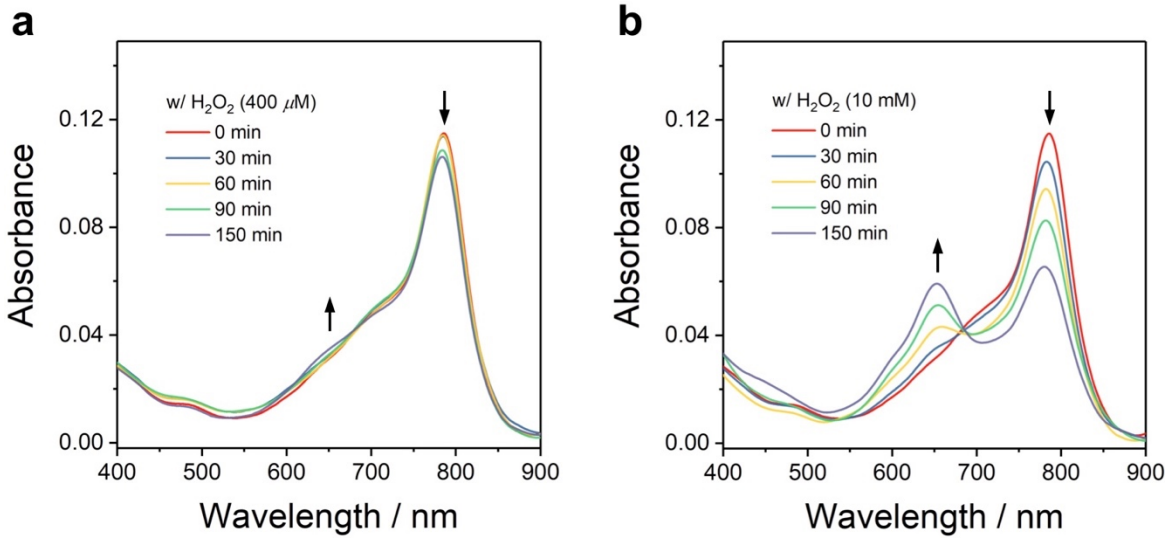

Figure S13. UV−visible absorption spectra recorded for **BD-PG$_{Me}$/P$_8$** (conc. 2.0 μM **BD-PG$_{Me}$**; 0.1 g/L **P$_8$**) upon incubation with (a) 200 and (b) 5000 equivalents of H_2O_2 for varying time intervals (0-150 min) at 37 °C.

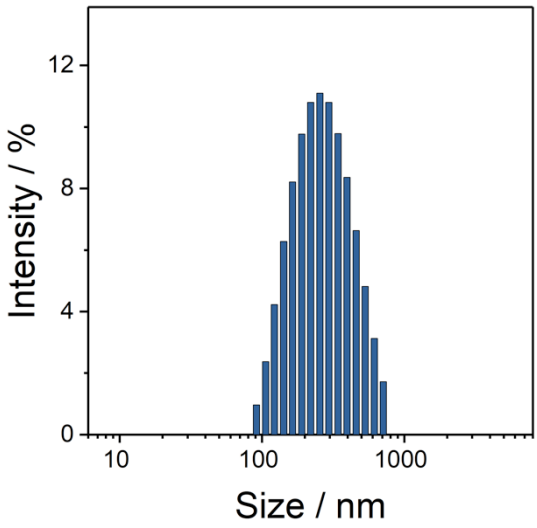

Figure S14. Size distribution of **BD-PG$_{Me}$/P$_8$** nano-assemblies (2.0% dye content) upon incubation with $OONO^-$ (5 equiv) for 30 min at 37 ^oC.

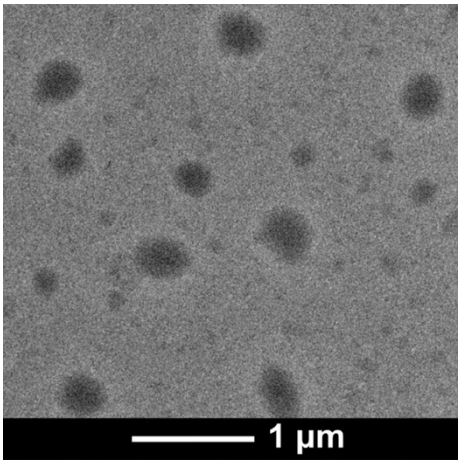

Figure S15. TEM image of ^{s}**BD-COOH$_{Me}$/P$_8$** nano-assemblies formed via self-assembly of **BD-COOH$_{Me}$** and **P$_8$** in aqueous solution.

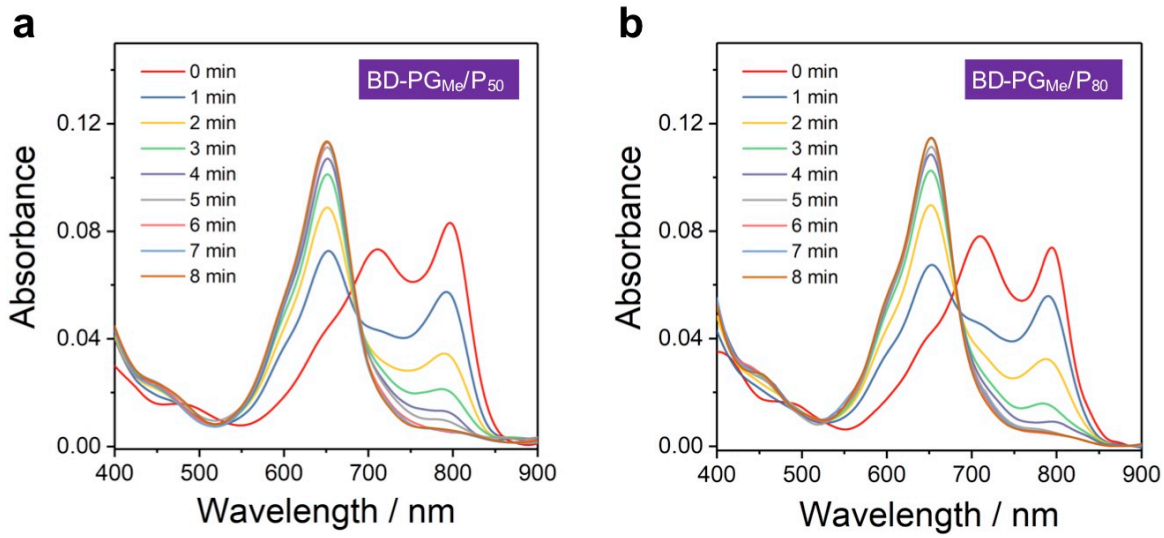

Figure S16. UV−visible absorption spectra recorded for (a) **BD-PG$_{Me}$/P$_{50}$** (conc. 2.0 μM **BD-PG$_{Me}$**; 0.1 g/L **P$_{50}$**) and (b) **BD-PG$_{Me}$/P$_{80}$** (conc. 2.0 μM **BD-PG$_{Me}$**; 0.1 g/L **P$_{80}$**) upon incubation with $OONO^-$ (10 μM) for varying time intervals at 37 °C.

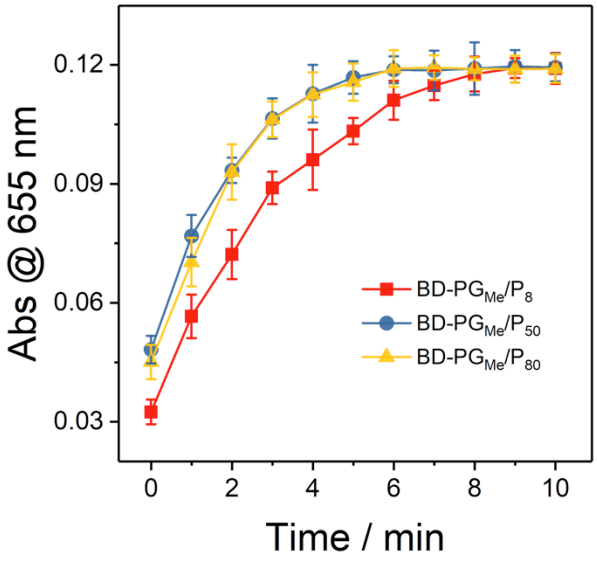

Figure S17. Plots of absorbance at 655 nm (Abs @ 655 nm) recorded for **BD-PG$_{Me}$/P$_8$** (red), **BD-PG$_{Me}$/P$_{50}$** (steel blue), and **BD-PG$_{Me}$/P$_{80}$** (yellow) upon incubation with $OONO^-$ (10 μM) for varying time intervals (0-10 min) at 37 °C. Conc. 2.0 μM **BD-PG$_{Me}$**; 0.1 g/L **P$_n$**. Error bars represent mean ± SD (n = 5).

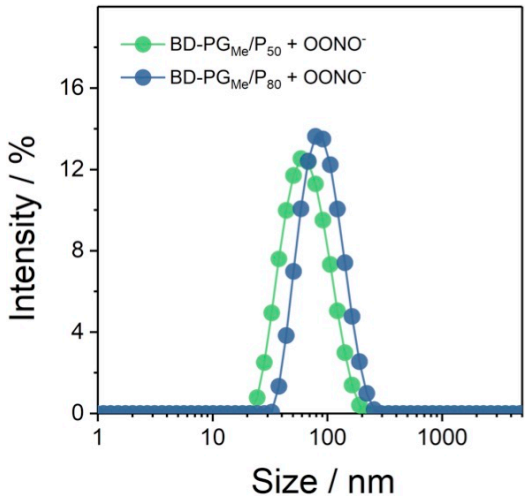

Figure S18. Size distribution of the aqueous solution of **BD-PG$_{Me}$/P$_{50}$** (green) and **BD-PG$_{Me}$/P$_{80}$** (steel blue) after incubation with $OONO^-$ (5 equivalent to **BD-PG$_{Me}$**) for 10 min at 37 °C using dynamic light scattering (DLS).

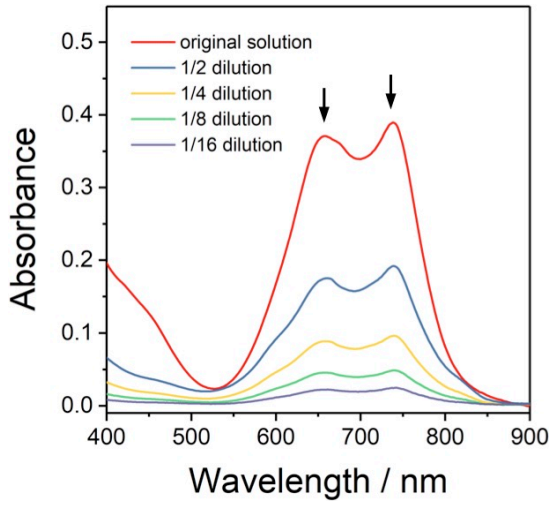

Figure S19. UV-visible absorption spectra recorded for $OONO^-$-treated **BD-PG$_{Me}$/P$_8$** solution following four 2-fold serial dilutions with PBS at 25 °C. The concentration of **P$_8$** in the original solution was 0.4 g/L, and the dye content was 3.4%.

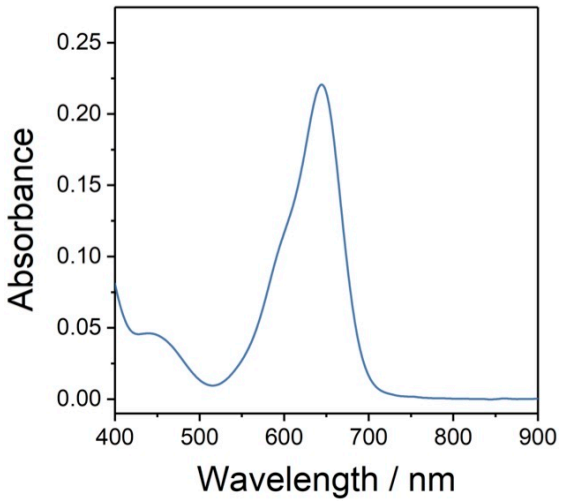

Figure S20. UV−visible absorption spectrum of 4.0 μM **BD-COOH$_{Me}$** in DMSO/water (8/2, v/v) mixture at 25 °C.

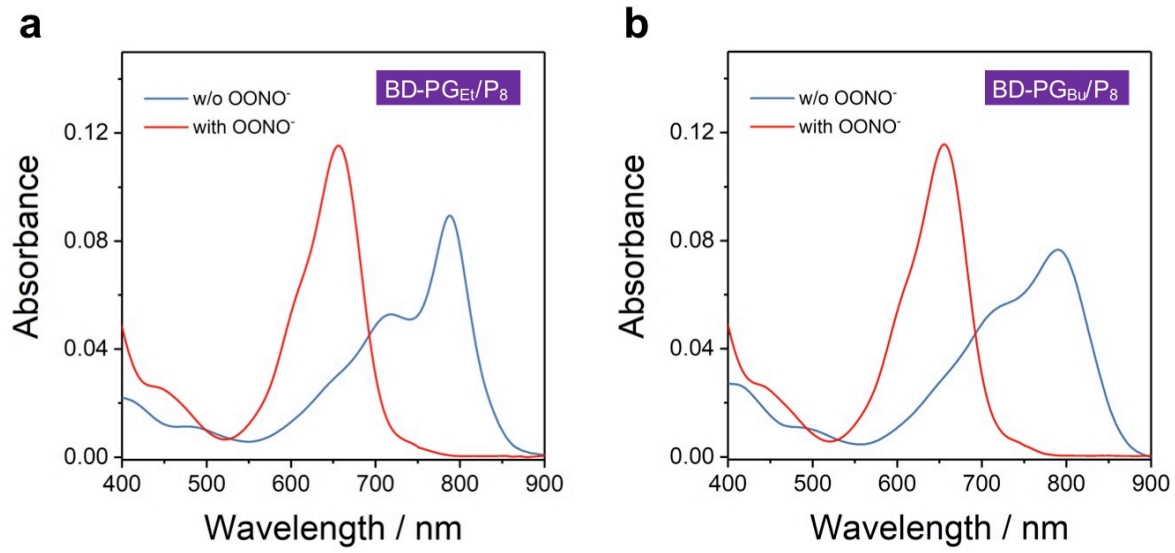

Figure S21. UV−visible absorption spectra recorded for (a) **BD-PG$_{Et}$/P$_8$** (conc: 2.0 μM **BD-PG$_{Et}$**; 0.1 g/L **P$_8$**) and (b) **BD-PG$_{Bu}$/P$_8$** (conc: 2.0 μM **BD-PG$_{Bu}$**; 0.1 g/L **P$_8$**) without (steel blue) or with (red) incubation with $OONO^-$ (10 μM) at 37 °C.

6.2 Photosensitivity assessment

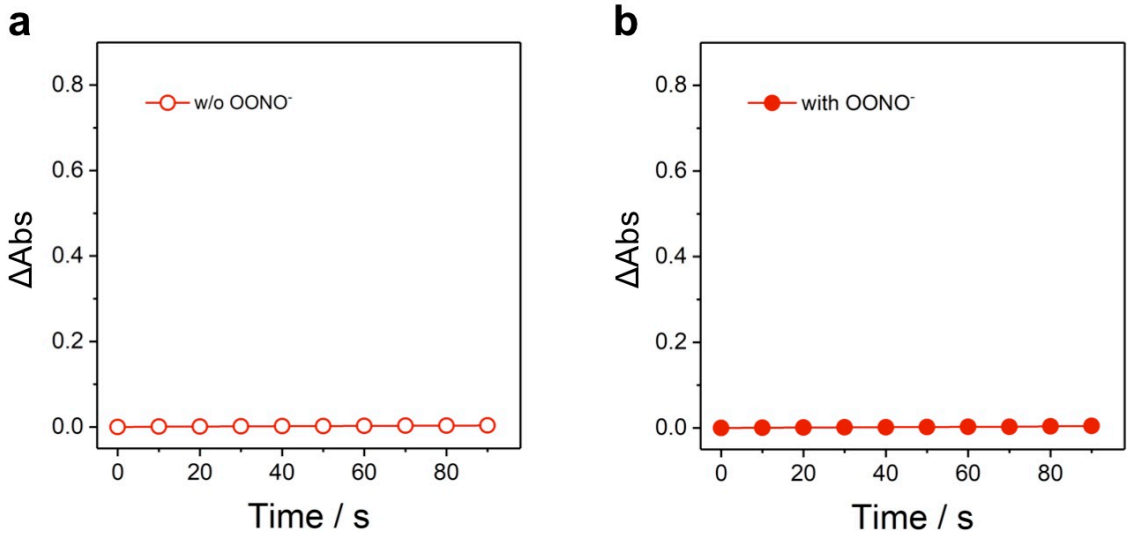

Figure S22. Plots of change in absorbance (ΔAbs) of QDPBF at 412 nm in dark for different time intervals in the presence of (a) untreated or (b) $OONO^-$-treated solution of **BD-PG$_{Me}$/P$_8$** at 37 °C. Conc. 1.0 μM **BD-PG$_{Me}$**; 0.05 g/L **P$_8$**.

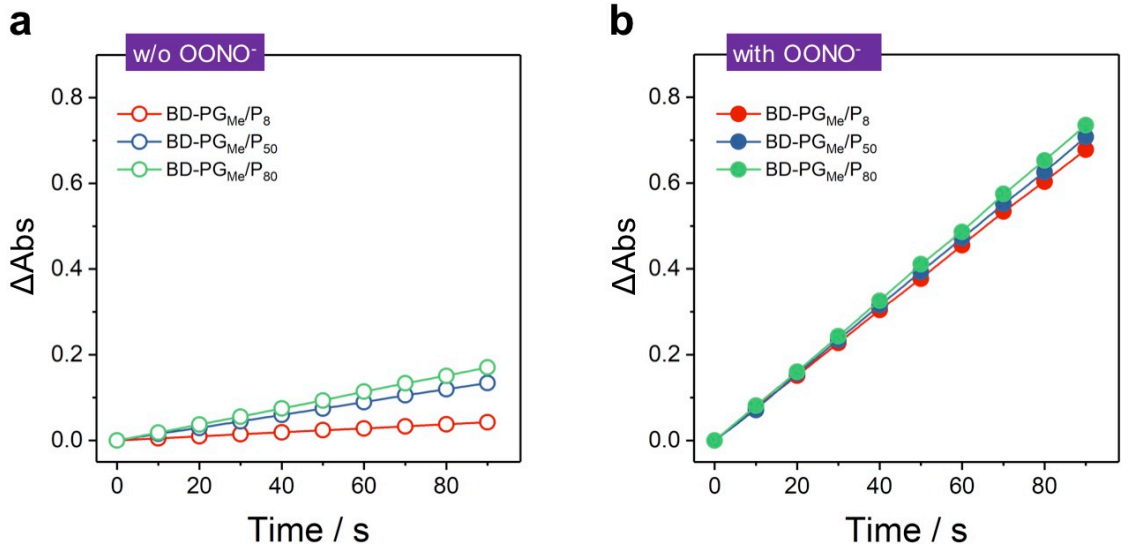

Figure S23. Plots of change in absorbance (ΔAbs) of QDPBF at 412 nm upon light irradiation at 655 nm (5 mW/cm^2) for different time intervals in the presence of (a) untreated or (b) $OONO^-$-treated solution of **BD-PG$_{Me}$/P$_8$** (red), **BD-PG$_{Me}$/P$_{50}$** (steel blue), and **BD-PG$_{Me}$/P$_{80}$** (green) at 37 °C. Conc. 1.0 μM **BD-PG$_{Me}$**; 0.05 g/L **P$_n$**.

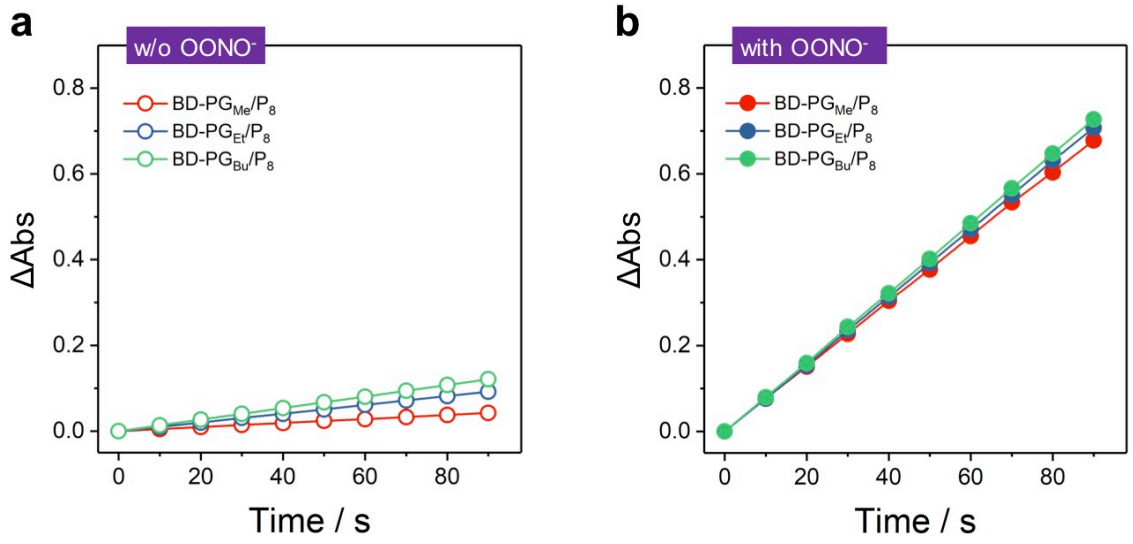

Figure S24. Plots of change in absorbance (ΔAbs) of QDPBF at 412 nm upon light irradiation at 655 nm (5 mW/cm^2) for different time intervals in the presence of (a) untreated or (b) $OONO^-$-treated solution of **BD-PG$_{Me}$/P$_8$** (red), **BD-PG$_{Et}$/P$_8$** (steel blue), and **BD-PG$_{Bu}$/P$_8$** (green) at 37 °C. Conc. 1.0 μM **BD-PG$_R$**; 0.05 g/L **P$_8$**.

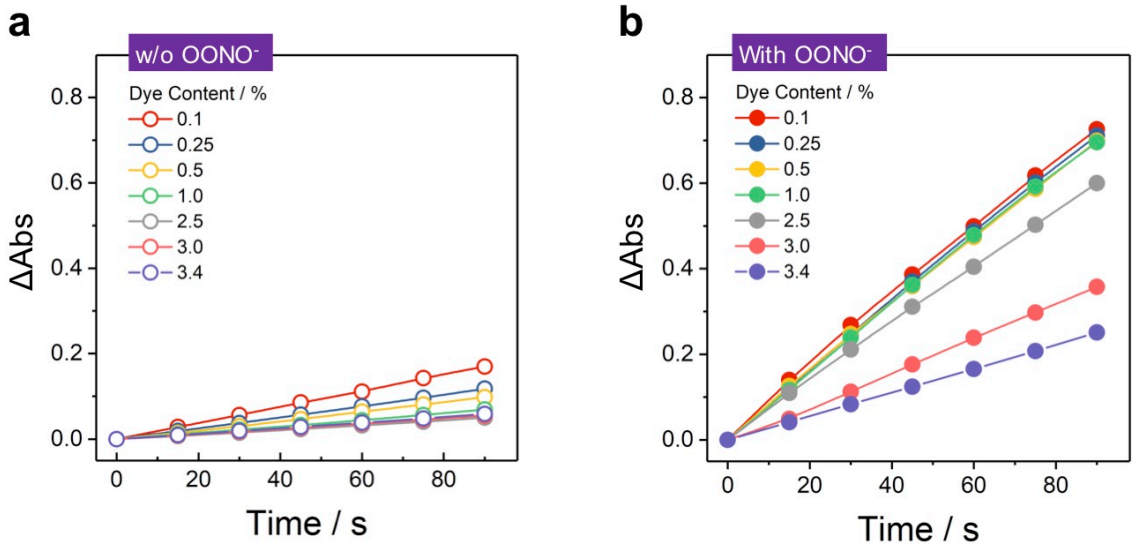

Figure S25. Plots of change in absorbance (ΔAbs) of QDPBF at 412 nm upon light irradiation at 655 nm (5 mW/cm^2) for different time intervals at 37 °C in the presence of (a) untreated or (b) $OONO^-$-treated solution of **BD-PG$_{Me}$/P$_8$** with different **BD-PG$_{Me}$** contents as indicated. The concentration of **BD-PG$_{Me}$** was fixed at 1.0 μM.

6.3 Fluorescence images, flow cytometric analyses, and MTT assay

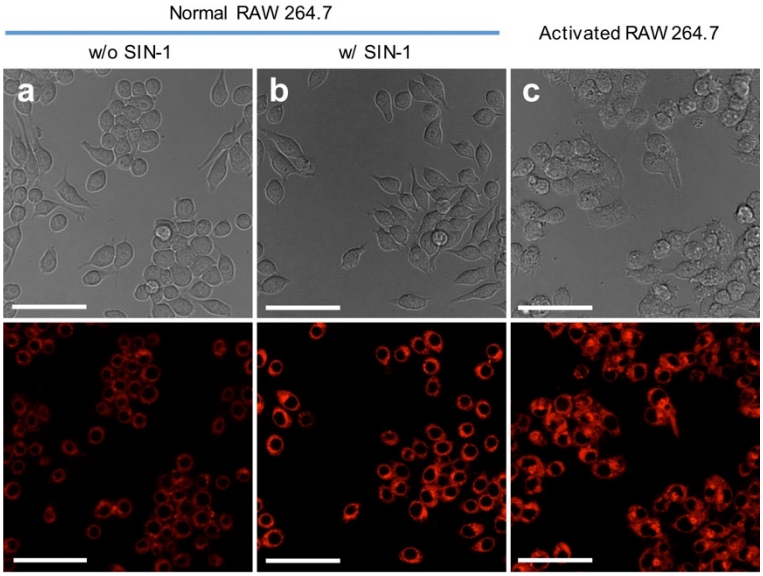

Figure S26. Confocal fluorescence images of normal RAW 264.7 cells pretreated without (a) or with (b) SIN-1, and activated RAW 264.7 cells (c) after incubation with ^{nano}**PS-PG** for 2 h at $\lambda_{ex/em}$ of 633/600-750 nm. Scale bars are 50 μm.

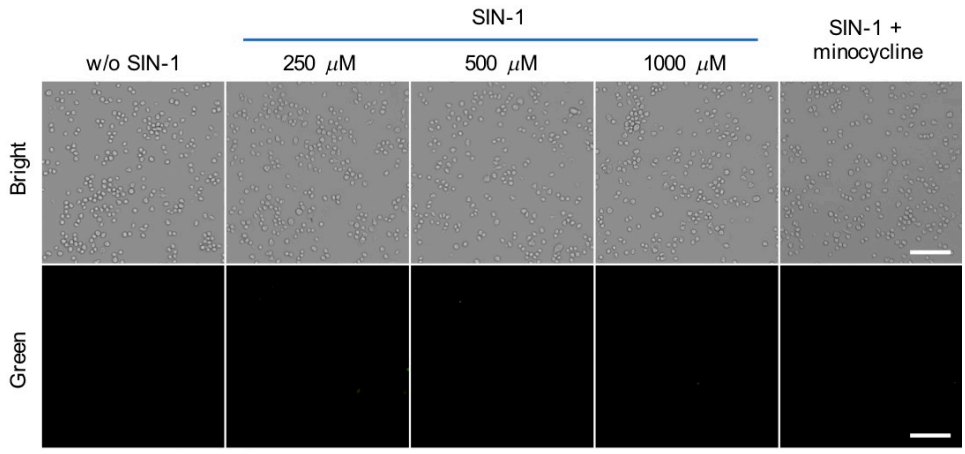

Figure S27. Intracellular ROS production using ROS probe DCF-DA. Cells were treated with ^{nano}**PS-PG** (containing 1.0 μM **BD-PG$_{Me}$**) for 30 min, and incubated with SIN-1 at different concentrations (first column: without SIN-1; second-fourth columns: 250, 500, 1000 μM SIN-1; last column: 1000 μM SIN-1 and 100 μM minocycline) for 2 h. After treatment, the control cell lines without light irradiation were stained with 10.0 μM DCF-DA for 20 min and imaged.

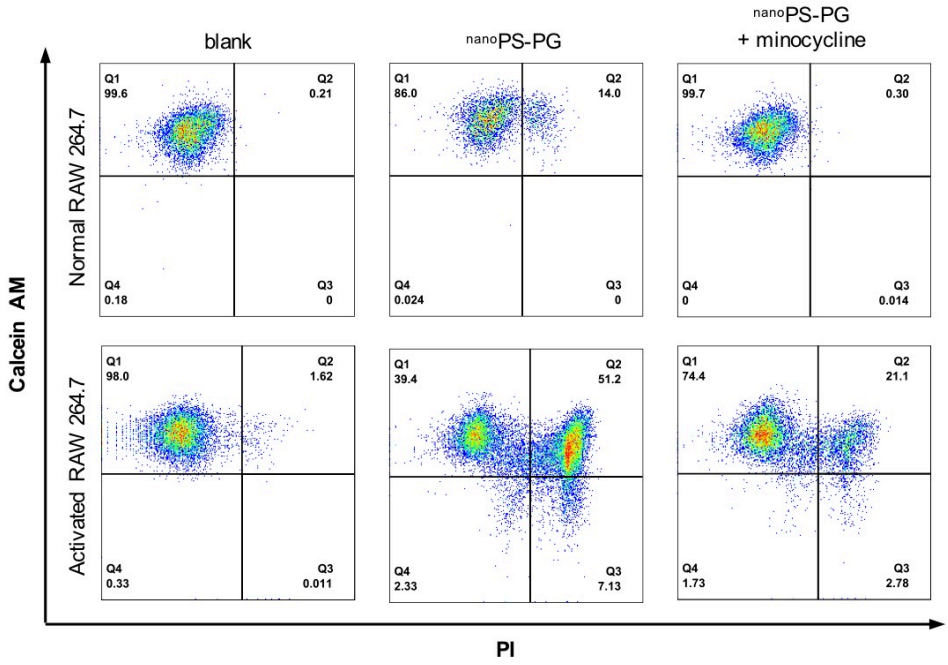

Figure S28. Flow cytometric analyses of normal (top line) and activated (bottom line) RAW 264.7 cells death induced by PDT. Cells were treated with **^{nano}PS-PG** (containing 1.0 μM **BD-PG$_{Me}$**) for 2 h followed by subjected to LED light irradiation (620-660 nm, 15 mW/cm^2) for 5 min. After treatment, the cells were incubated for 4 h and then stained with 1.0 μM Calcein AM (live staining, green) and 6.0 μM PI (dead staining, red) for 20 min. left: blank; middle: **^{nano}PS-PG** (containing 1.0 μM **BD-PG$_{Me}$**); right: **^{nano}PS-PG** (containing 1.0 μM **BD-PG$_{Me}$**) and 100 μM minocycline.

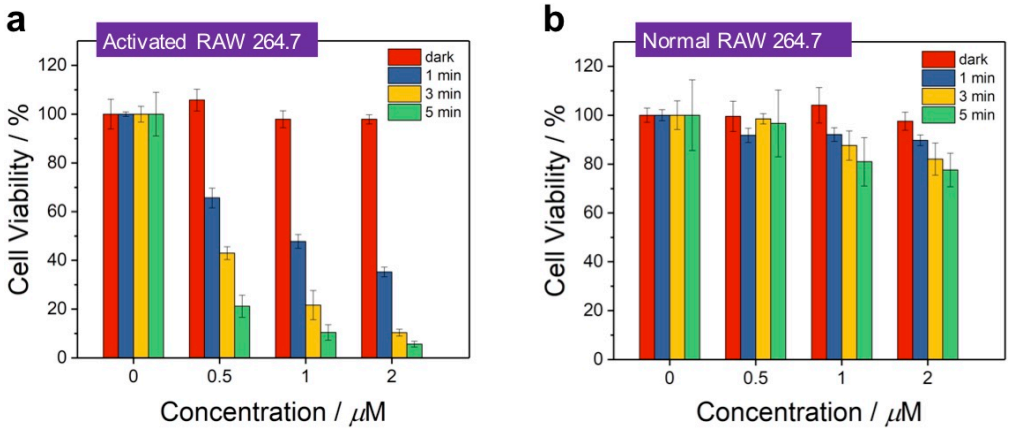

Figure S29. Cell viability was measured by MTT assay. Activated (a) and normal (b) RAW 264.7 cells were treated without or with **^{nano}PS-PG** (containing 1.0 μM **BD-PG$_{Me}$**) at various concentrations of **BD-PG$_{Me}$** as indicated for 2 h, and cell viability was measured without light irradiation (dark), or upon LED light irradiation (620-660 nm, 15 mW/cm^2) for 1, 3, or 5 min. Error bars represent mean ± SD (n = 5).

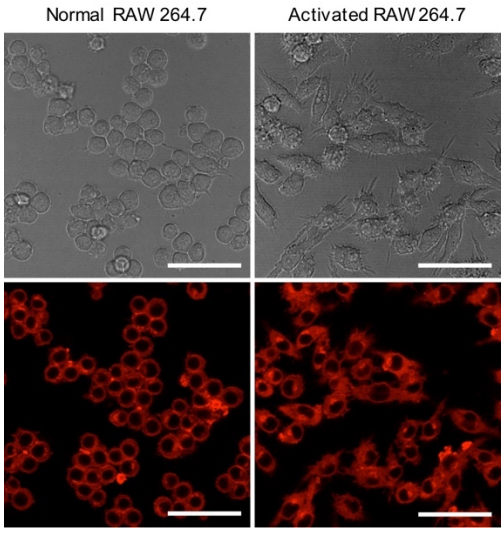

Figure S30. Confocal fluorescence images of normal RAW 264.7 cells (a) and activated RAW 264.7 cells (b) after incubation with ^{nano}**PS** for 2 h at $\lambda_{ex/em}$ of 633/600-750 nm. Scale bars are 50 μm.

7. NMR and HRMS spectra

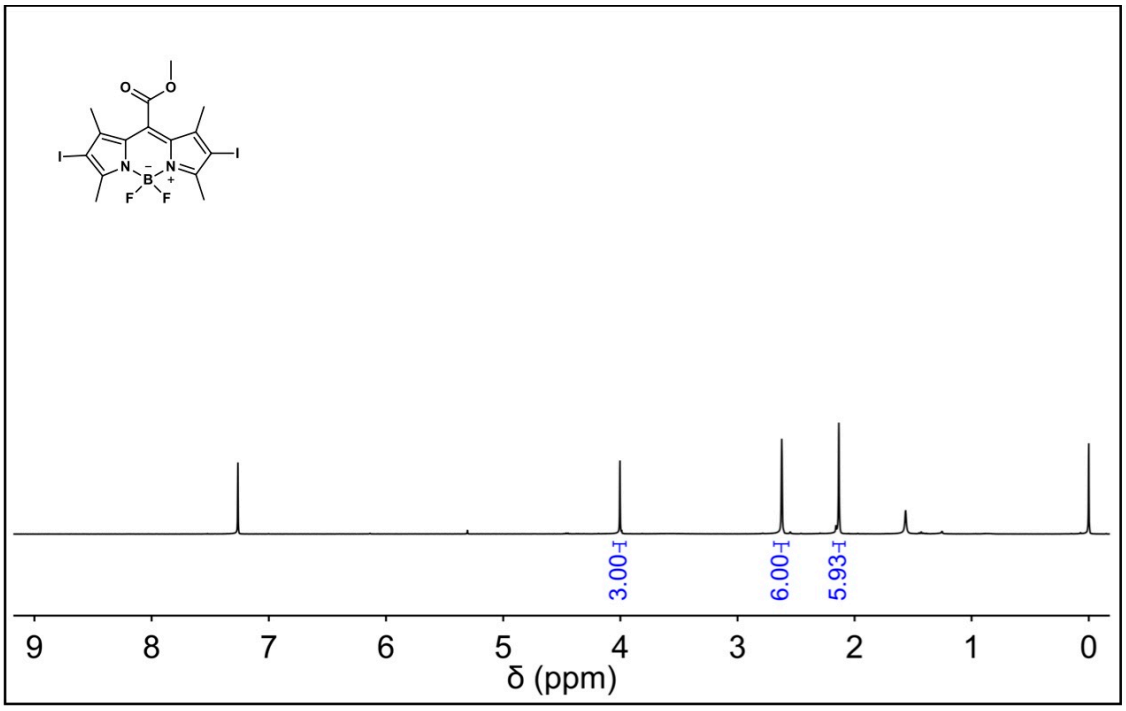

Figure S31. ^{1}H NMR spectrum (400 MHz) of compound **2** in $CDCl_3$ at 25 ºC.

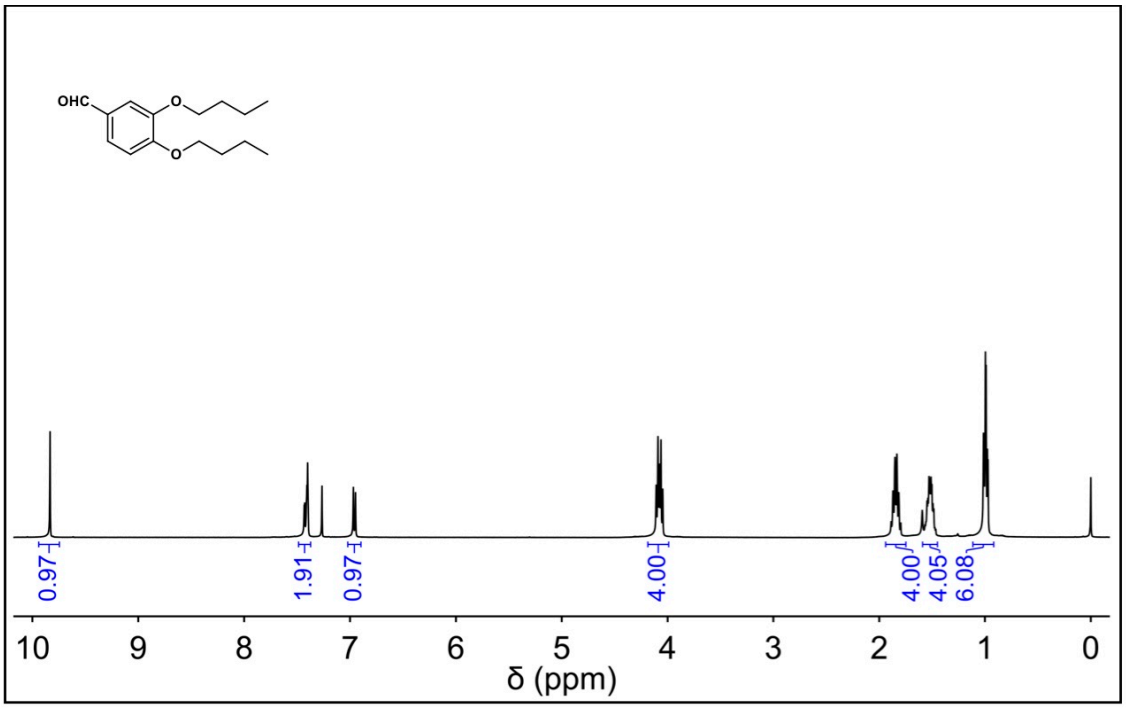

Figure S32. ^{1}H NMR spectrum (400 MHz) of compound **3c** in $CDCl_3$ at 25 ºC.

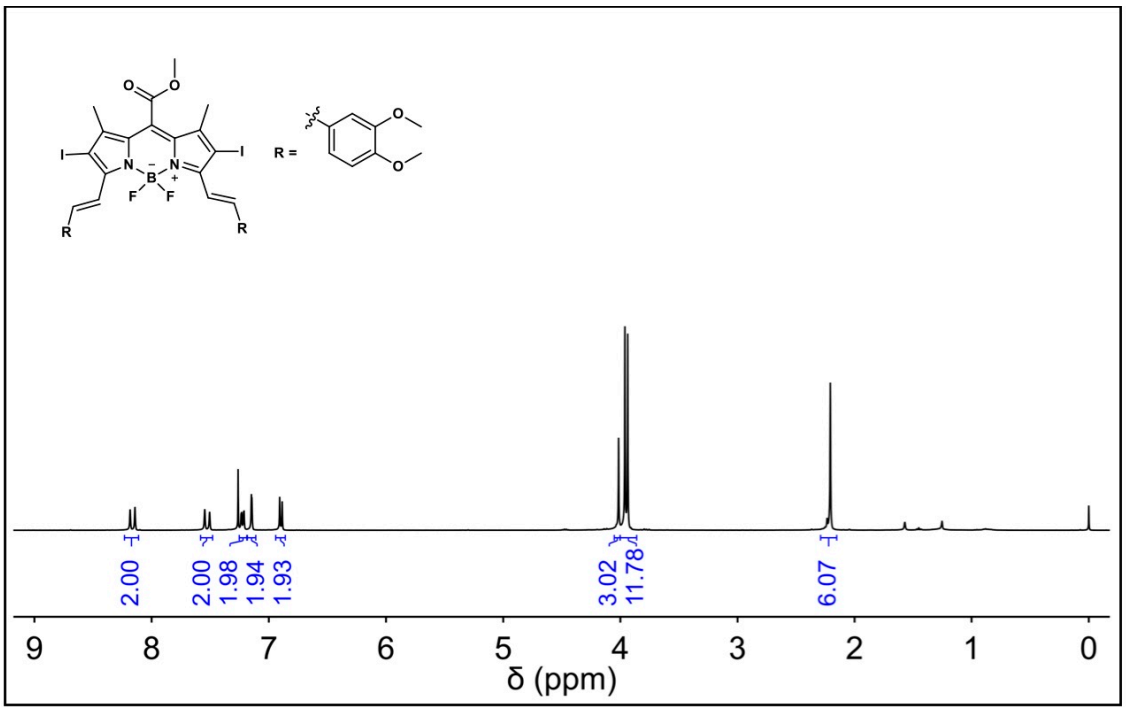

Figure S33. ^{1}H NMR spectrum (400 MHz) of compound **4a** in $CDCl_3$ at 25 ºC.

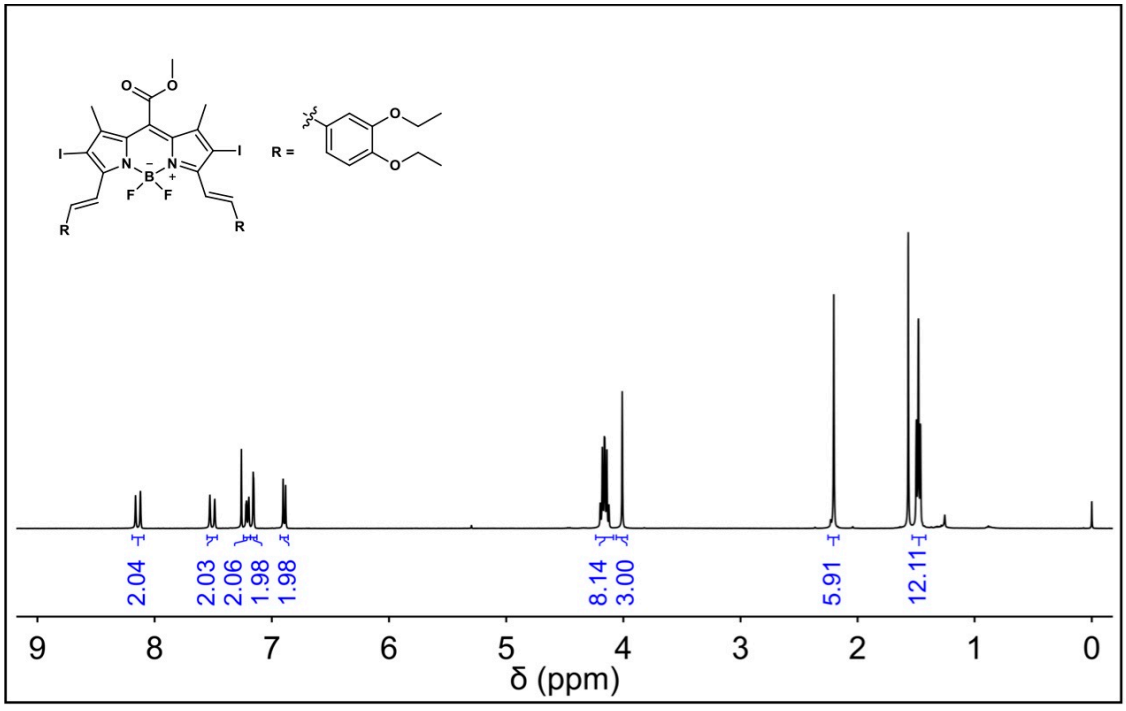

Figure S34. ^{1}H NMR spectrum (400 MHz) of compound **4b** in $CDCl_3$ at 25 ºC.

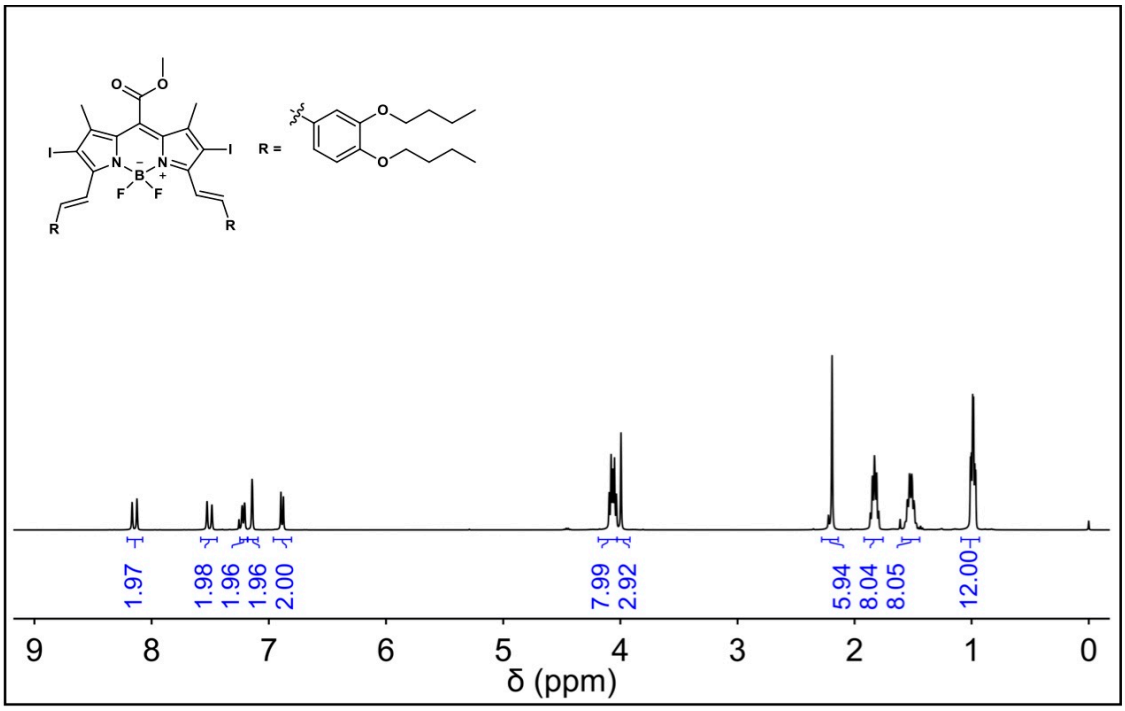

Figure S35. ^{1}H NMR spectrum (400 MHz) of compound **4c** in $CDCl_3$ at 25 ºC.

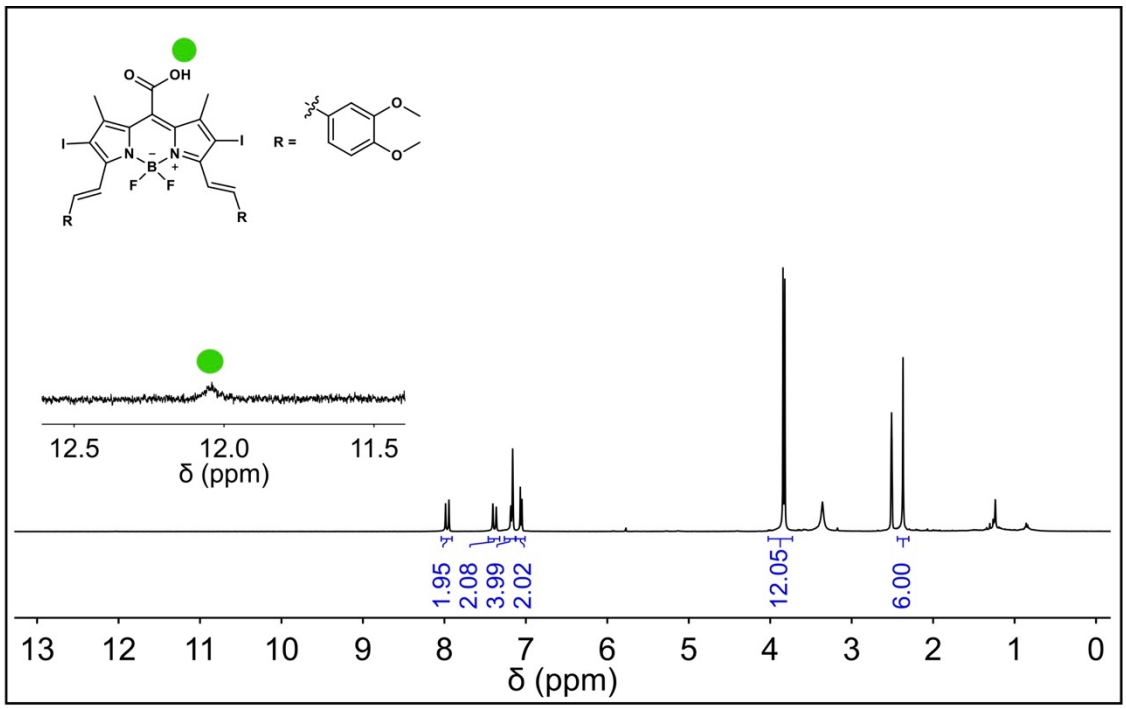

Figure S36. ^{1}H NMR spectrum (400 MHz) of compound **BD-COOH$_{Me}$** in DMSO-d_6 at 25 ºC.

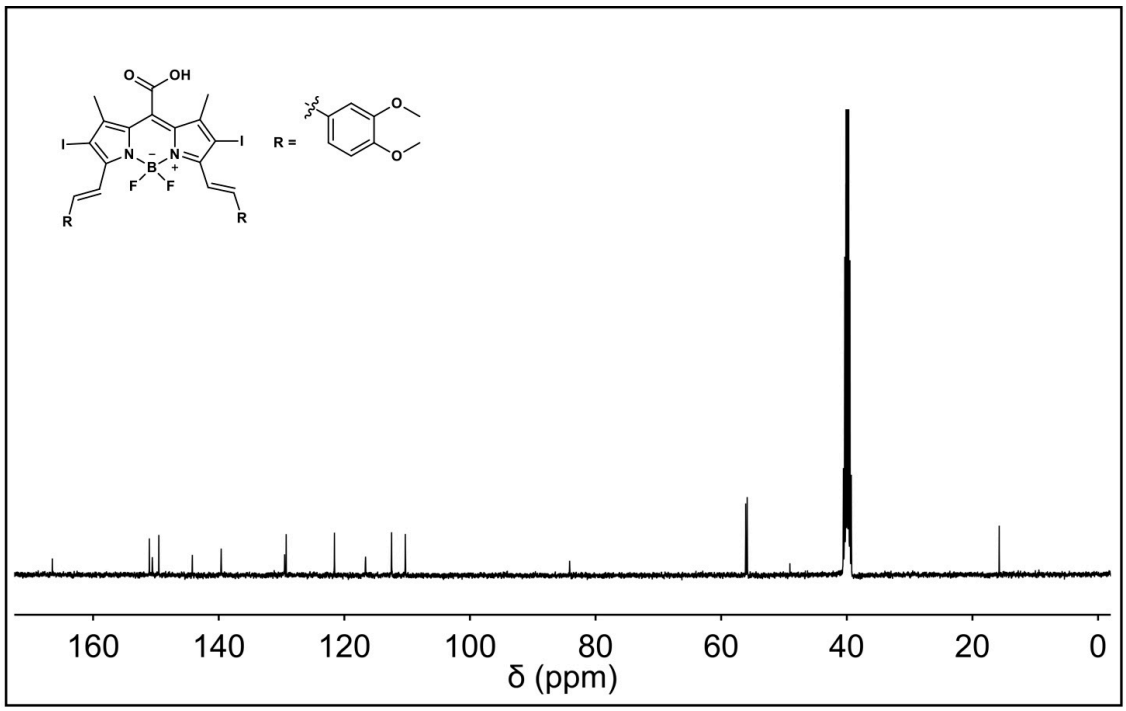

Figure S37. ^{13}C NMR spectrum (100 MHz) of compound **BD-COOH$_{Me}$** in DMSO-d_6 at 25 ºC.

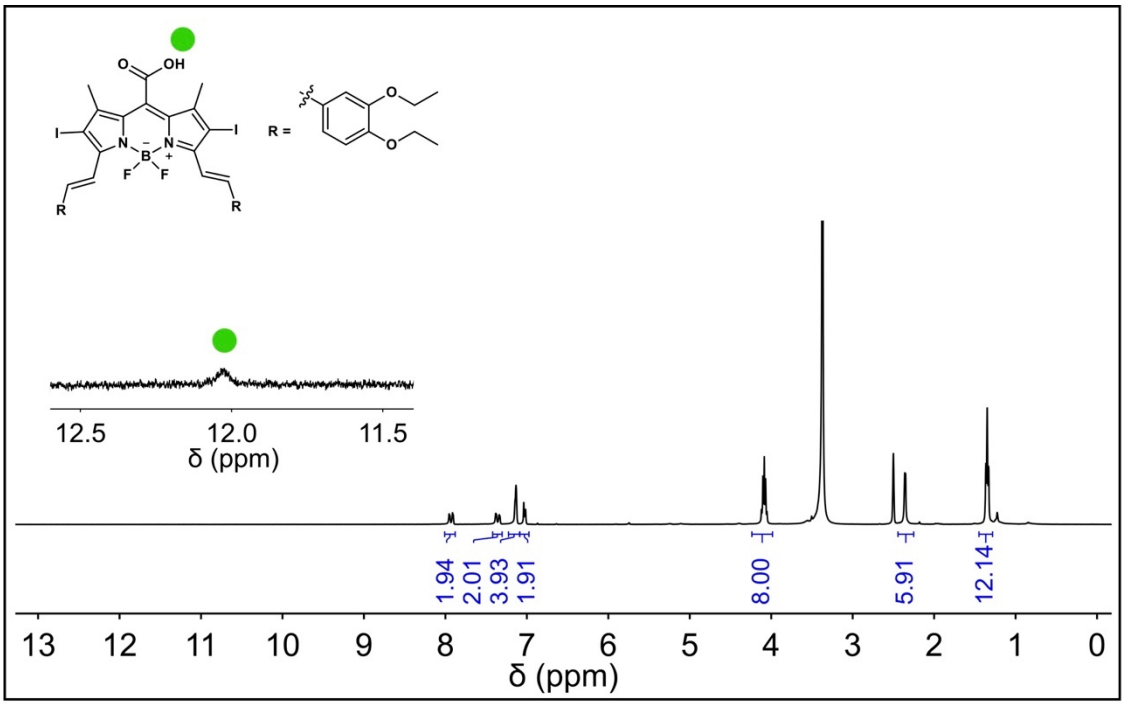

Figure S38. ^{1}H NMR spectrum (400 MHz) of compound **BD-COOH$_{Et}$** in DMSO-d_6 at 25 ºC.

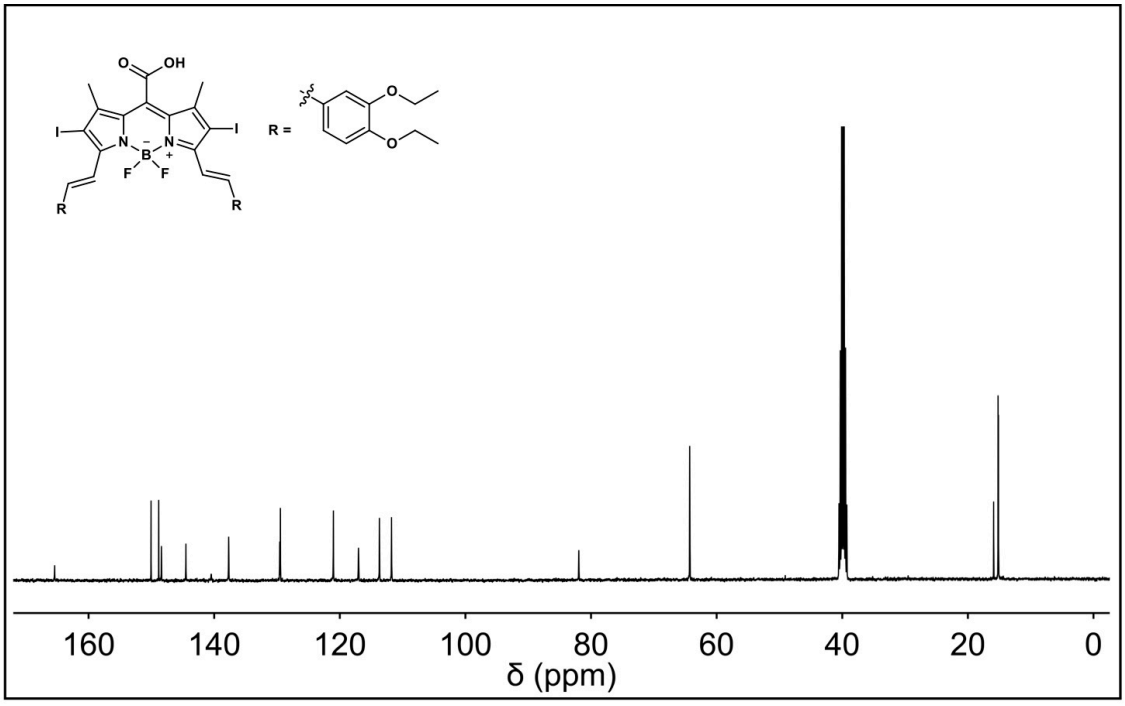

Figure S39. ^{13}C NMR spectrum (100 MHz) of compound **BD-COOH$_{Et}$** in DMSO-d_6 at 25 ºC.

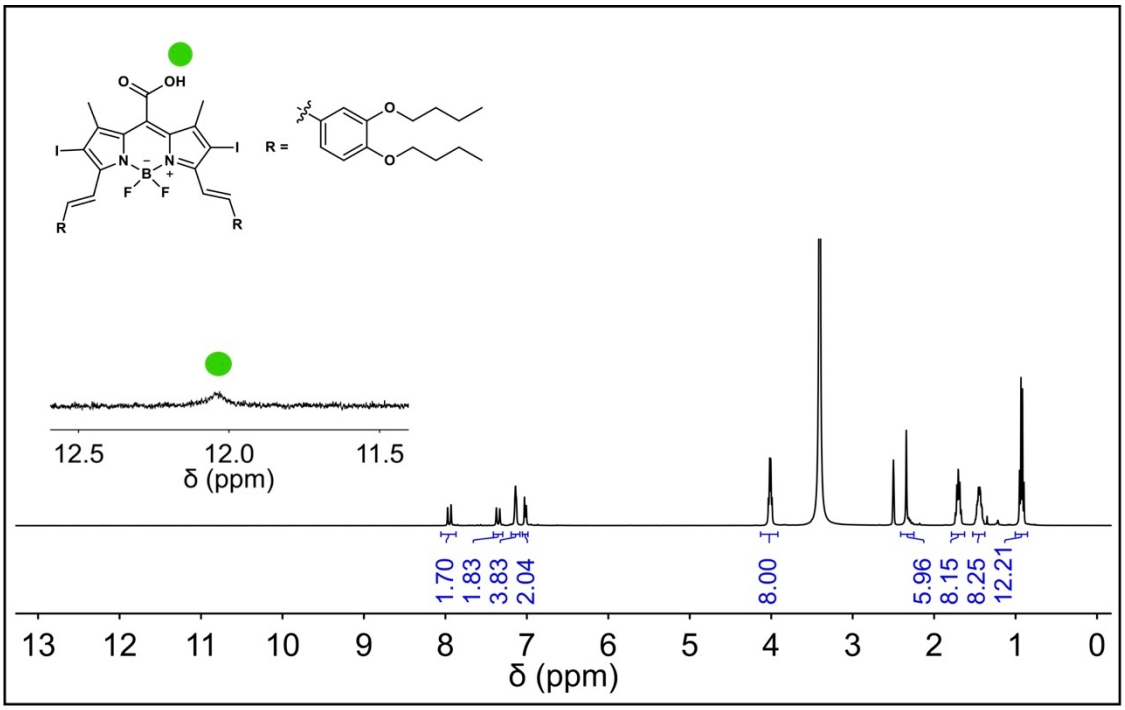

Figure S40. ^{1}H NMR spectrum (400 MHz) of compound **BD-COOH$_{Bu}$** in DMSO-d_6 at 25 ºC.

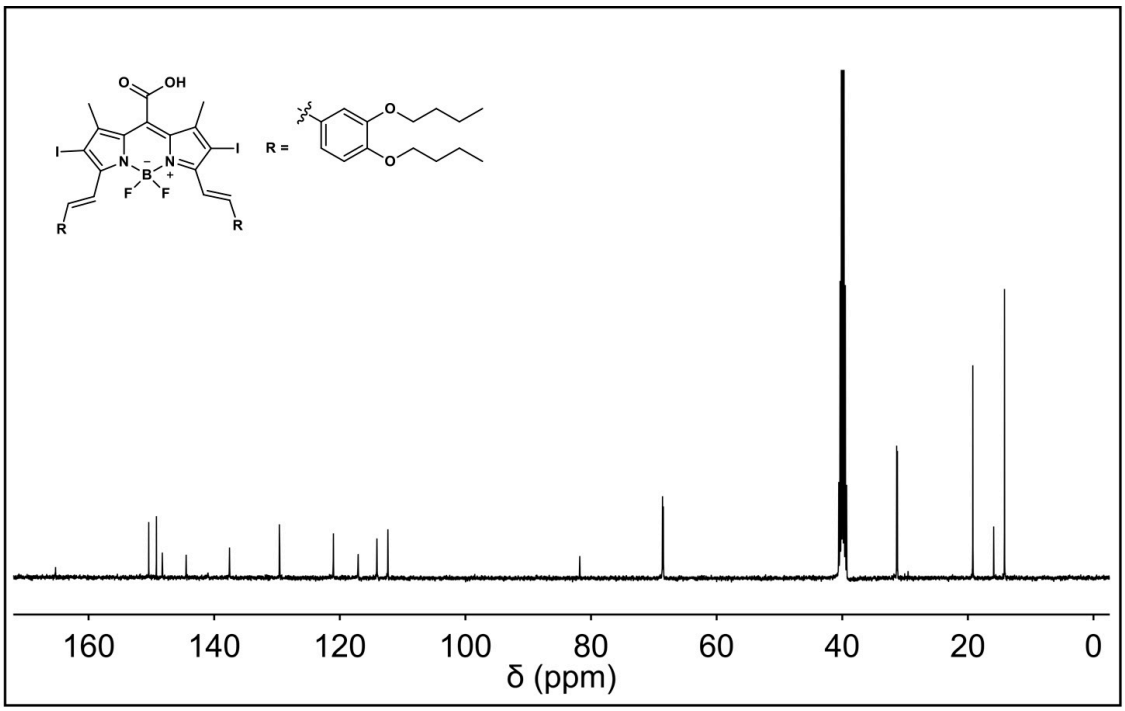

Figure S41. ^{13}C NMR spectrum (100 MHz) of compound **BD-COOH$_{Bu}$** in DMSO-d_6 at 25 ºC.

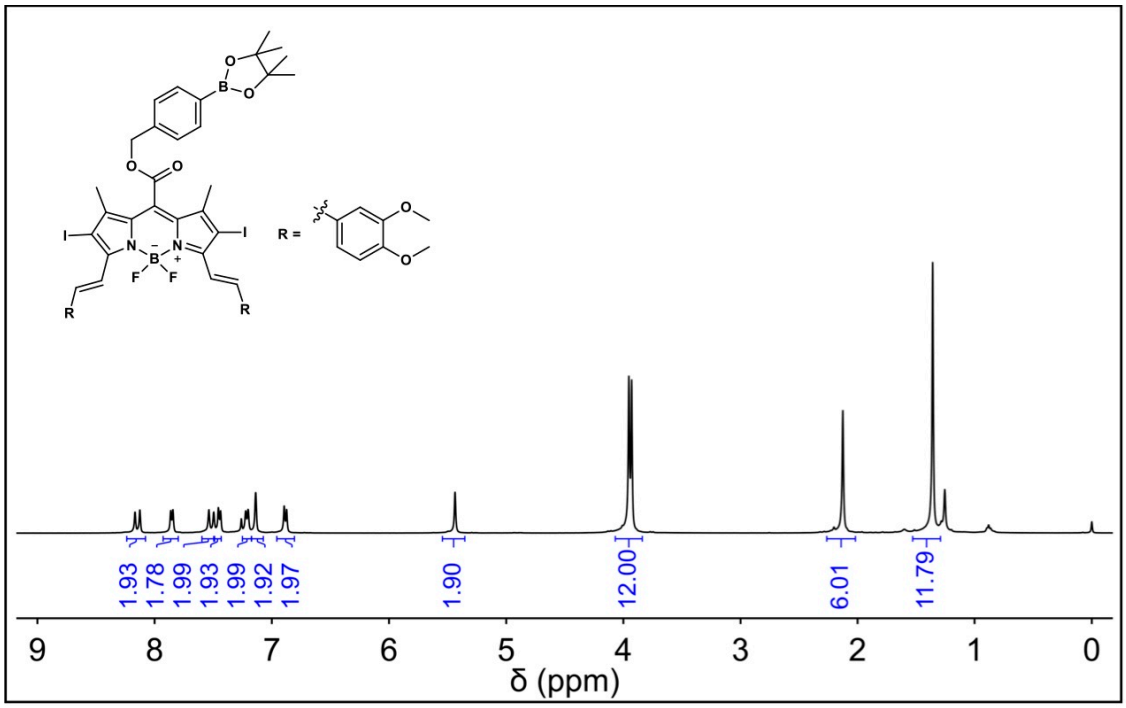

Figure S42. ^{1}H NMR spectrum (400 MHz) of compound **BD-PG$_{Me}$** in $CDCl_3$ at 25 ºC.

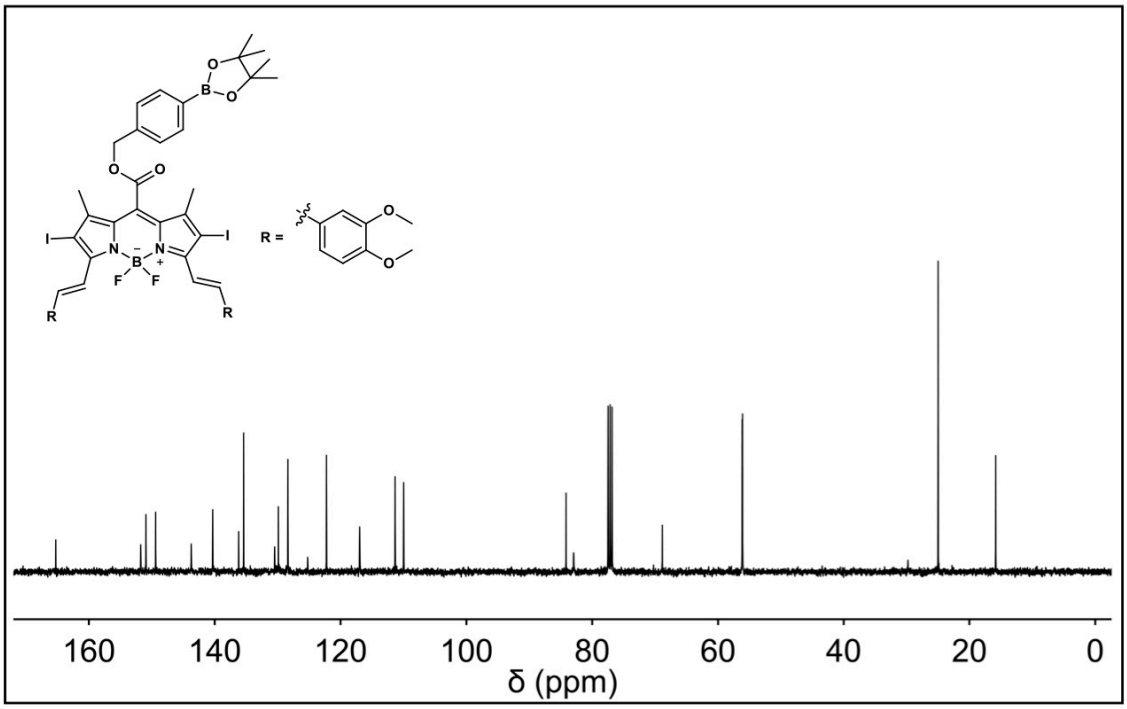

Figure S43. ^{13}C NMR spectrum (100 MHz) of compound **BD-PG$_{Me}$** in $CDCl_3$ at 25 ºC.

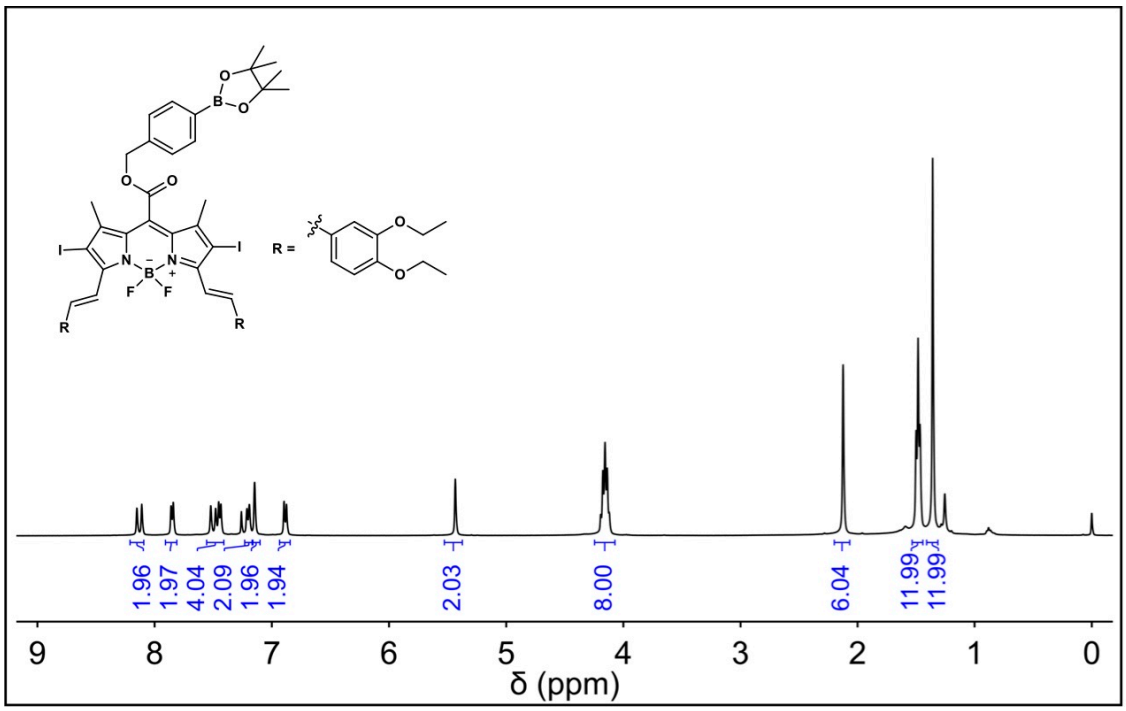

Figure S44. ^{1}H NMR spectrum (400 MHz) of compound **BD-PG$_{Et}$** in $CDCl_3$ at 25 ºC.

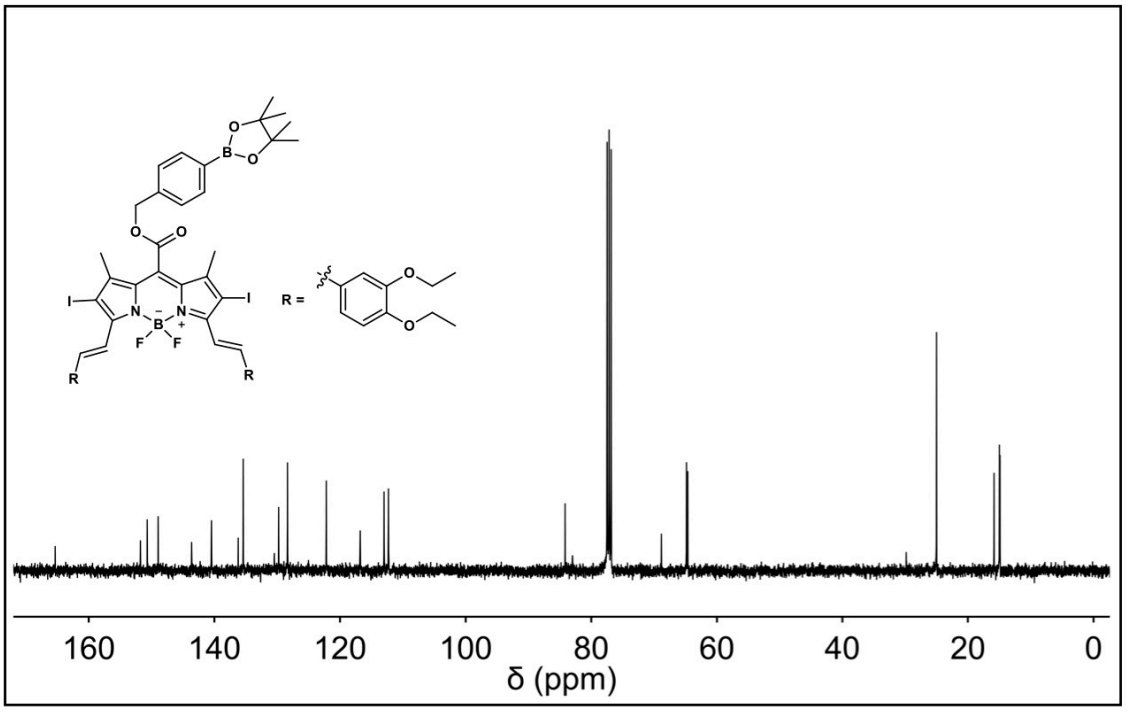

Figure S45. ^{13}C NMR spectrum (100 MHz) of compound **BD-PG$_{Et}$** in $CDCl_3$ at 25 ºC.

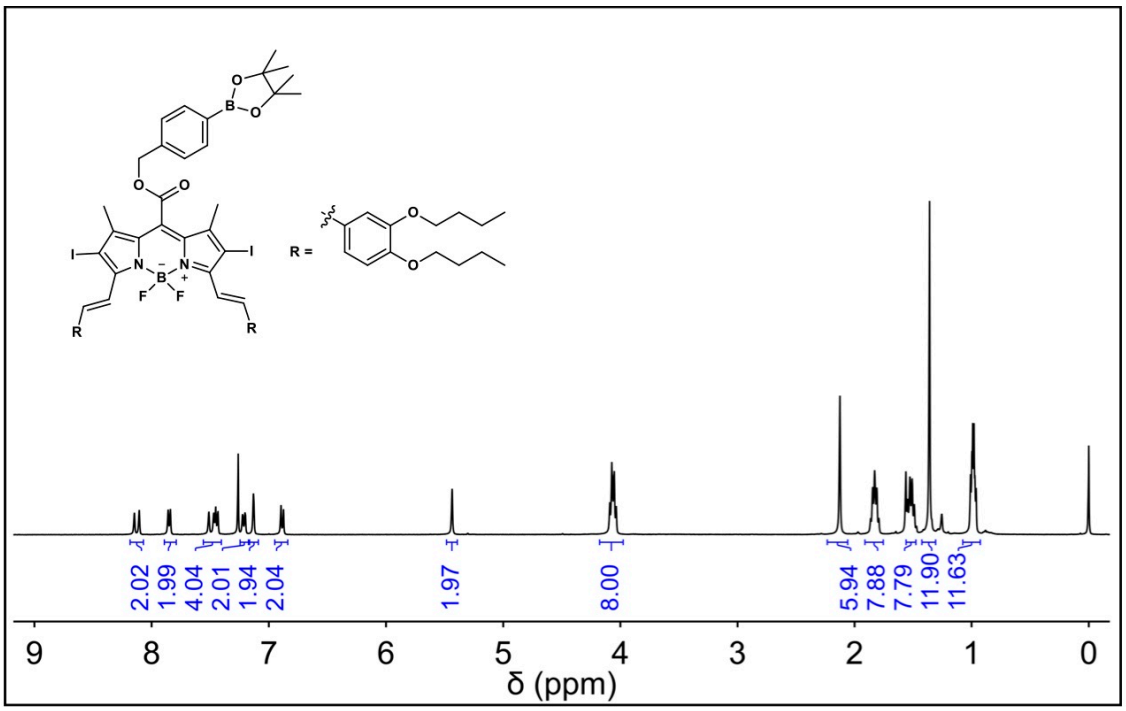

Figure S46. ^{1}H NMR spectrum (400 MHz) of compound **BD-PG$_{Bu}$** in $CDCl_3$ at 25 ºC.

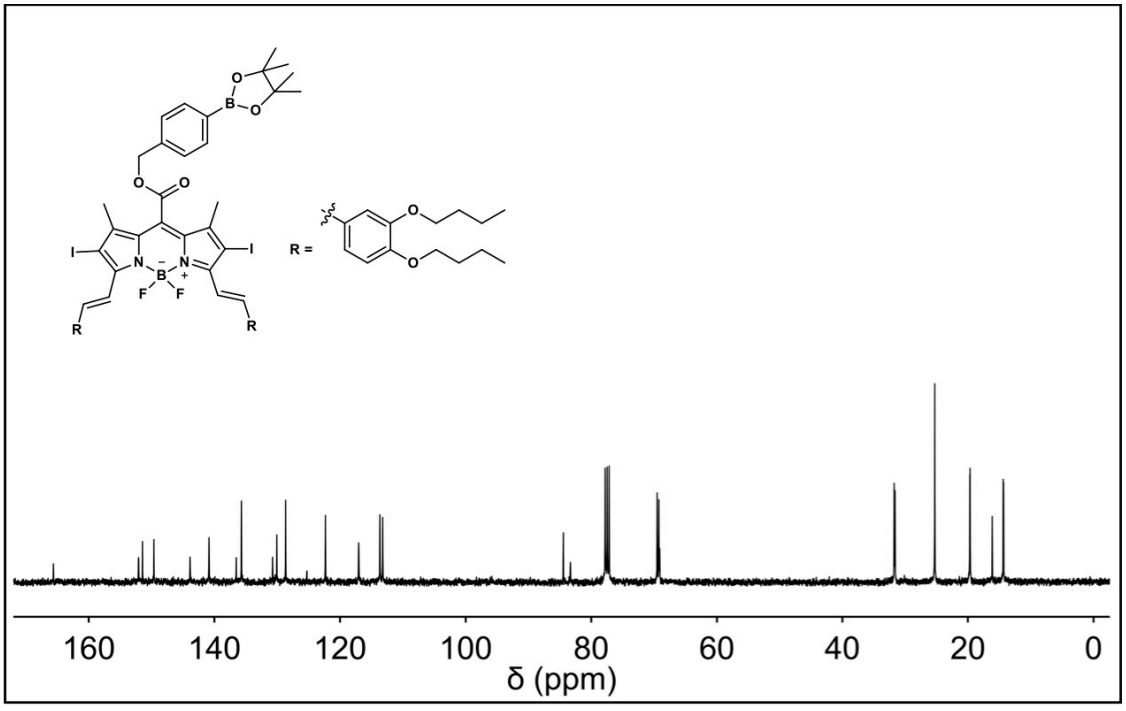

Figure S47. ^{13}C NMR spectrum (100 MHz) of compound **BD-PG$_{Bu}$** in $CDCl_3$ at 25 ºC.

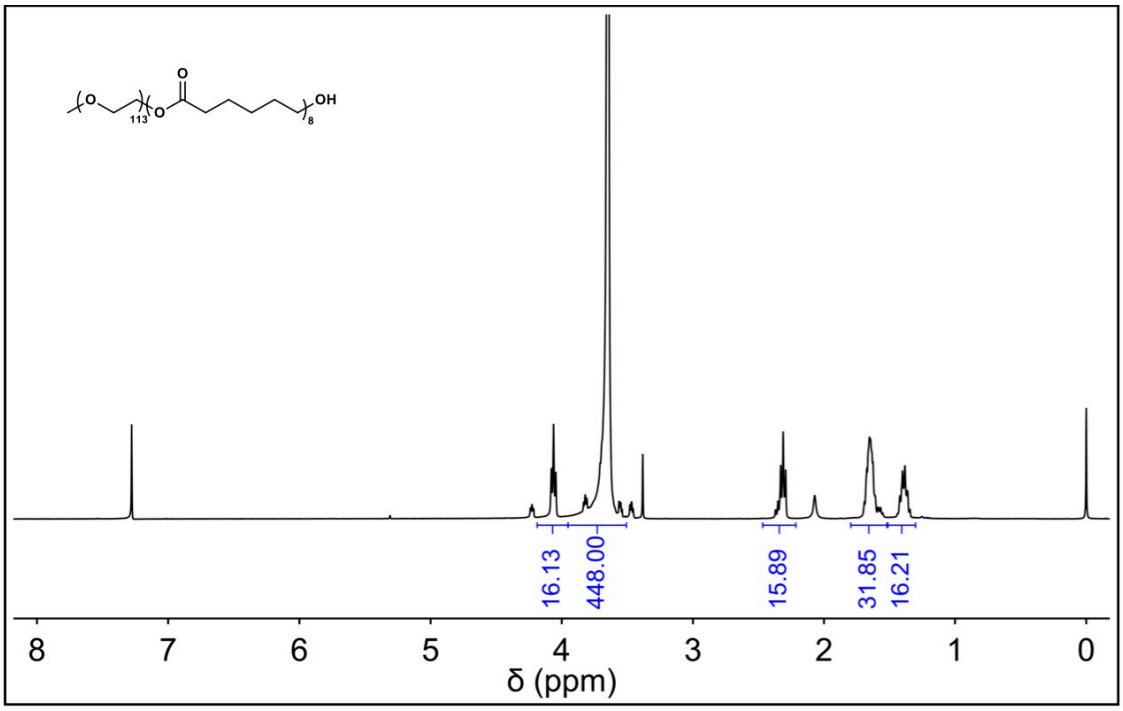

Figure S48. ^{1}H NMR spectrum (400 MHz) of compound $\mathbf{P_8}$ in $CDCl_3$ at 25 ºC.

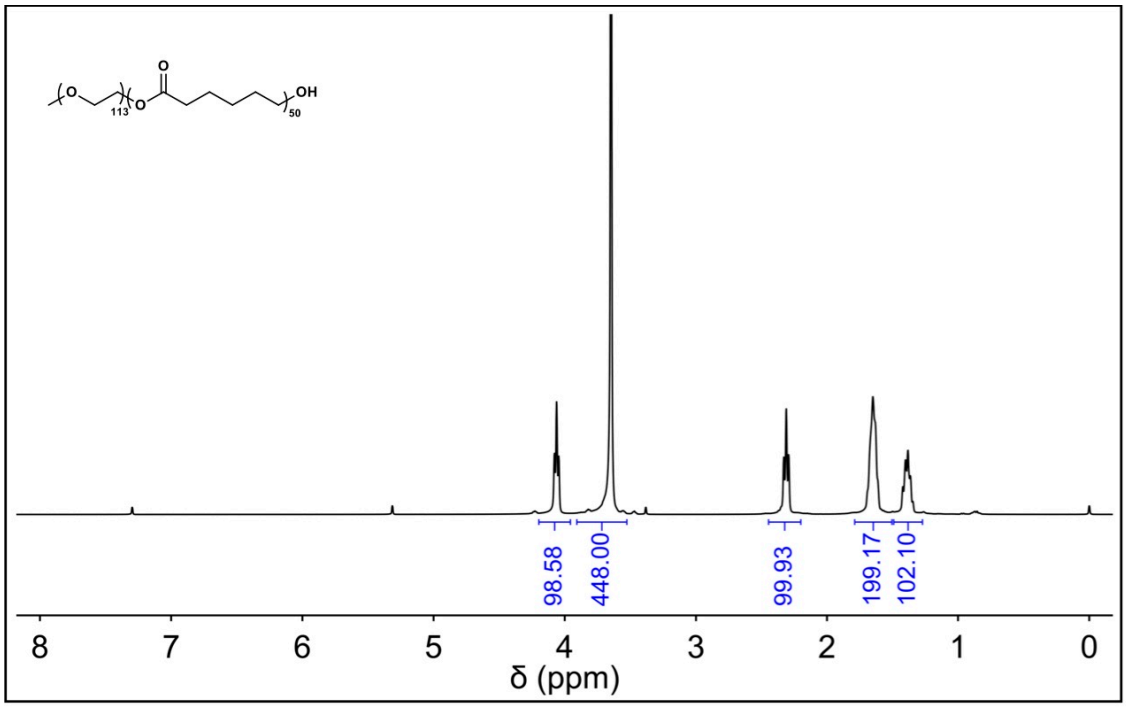

Figure S49. ^{1}H NMR spectrum (400 MHz) of compound $\mathbf{P_{50}}$ in $CDCl_3$ at 25 ºC.

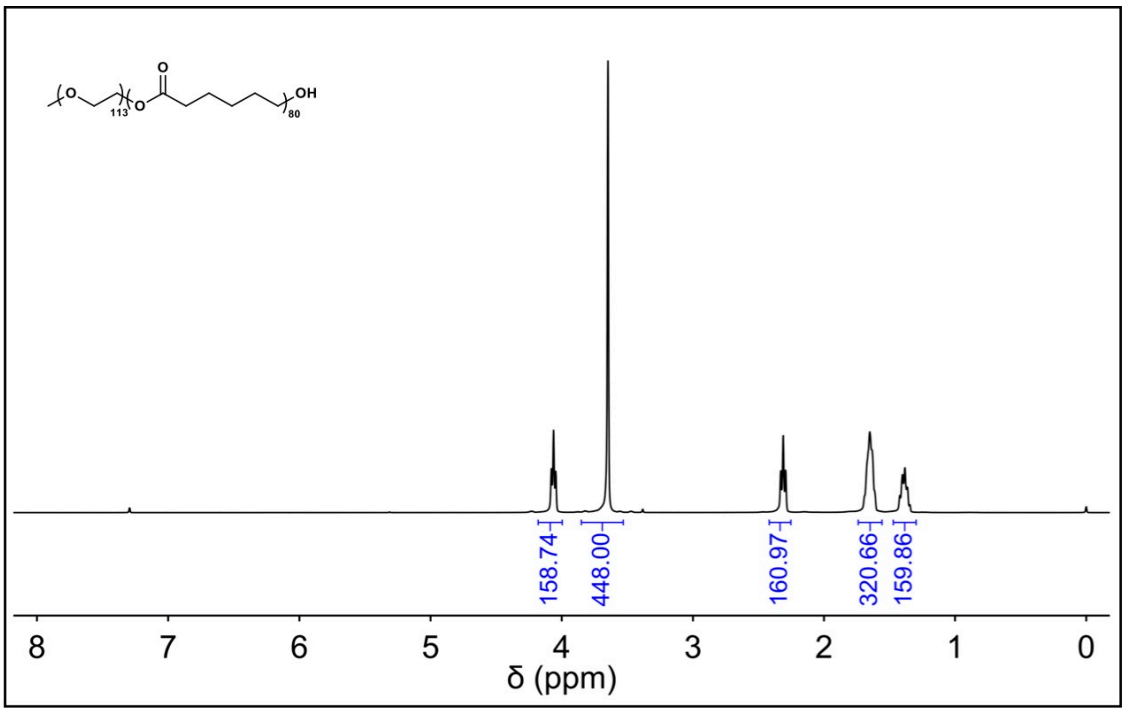

Figure S50. ^{1}H NMR spectrum (400 MHz) of compound $\mathbf{P_{80}}$ in $CDCl_3$ at 25 ºC.

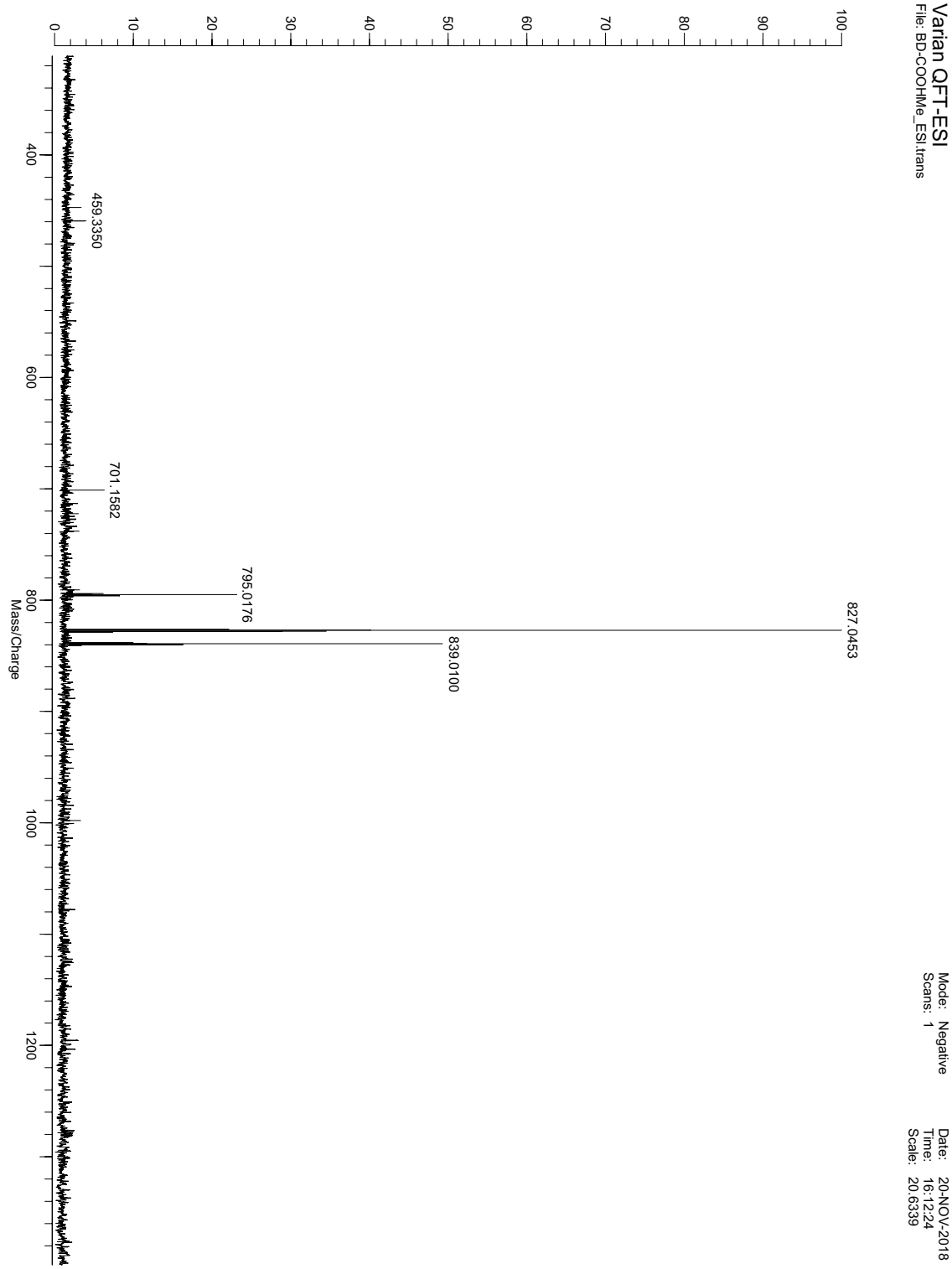

Figure S51. HRMS of **BD-COOH$_{Me}$**.

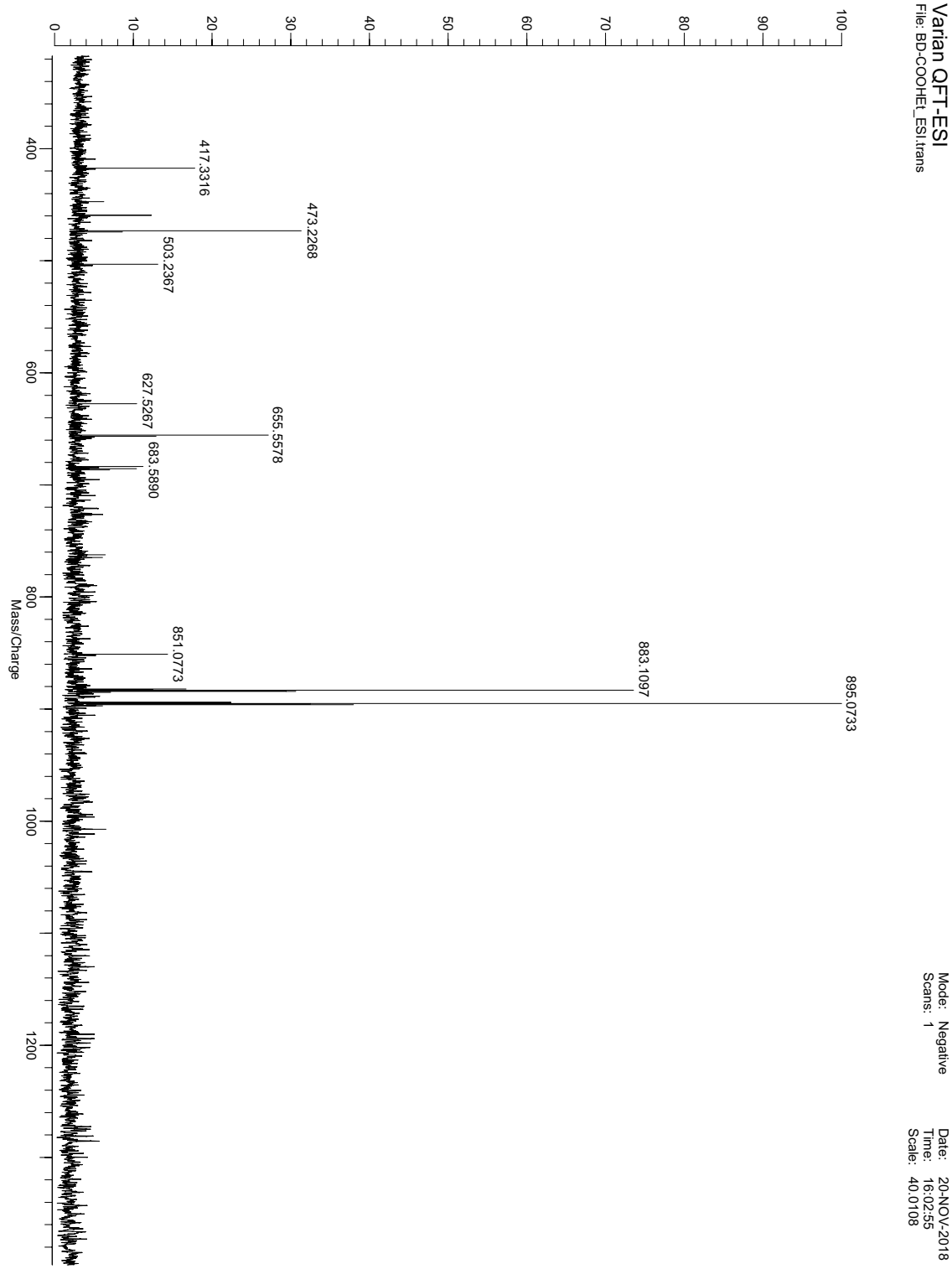

Figure S52. HRMS of **BD-COOH$_{Et}$**.

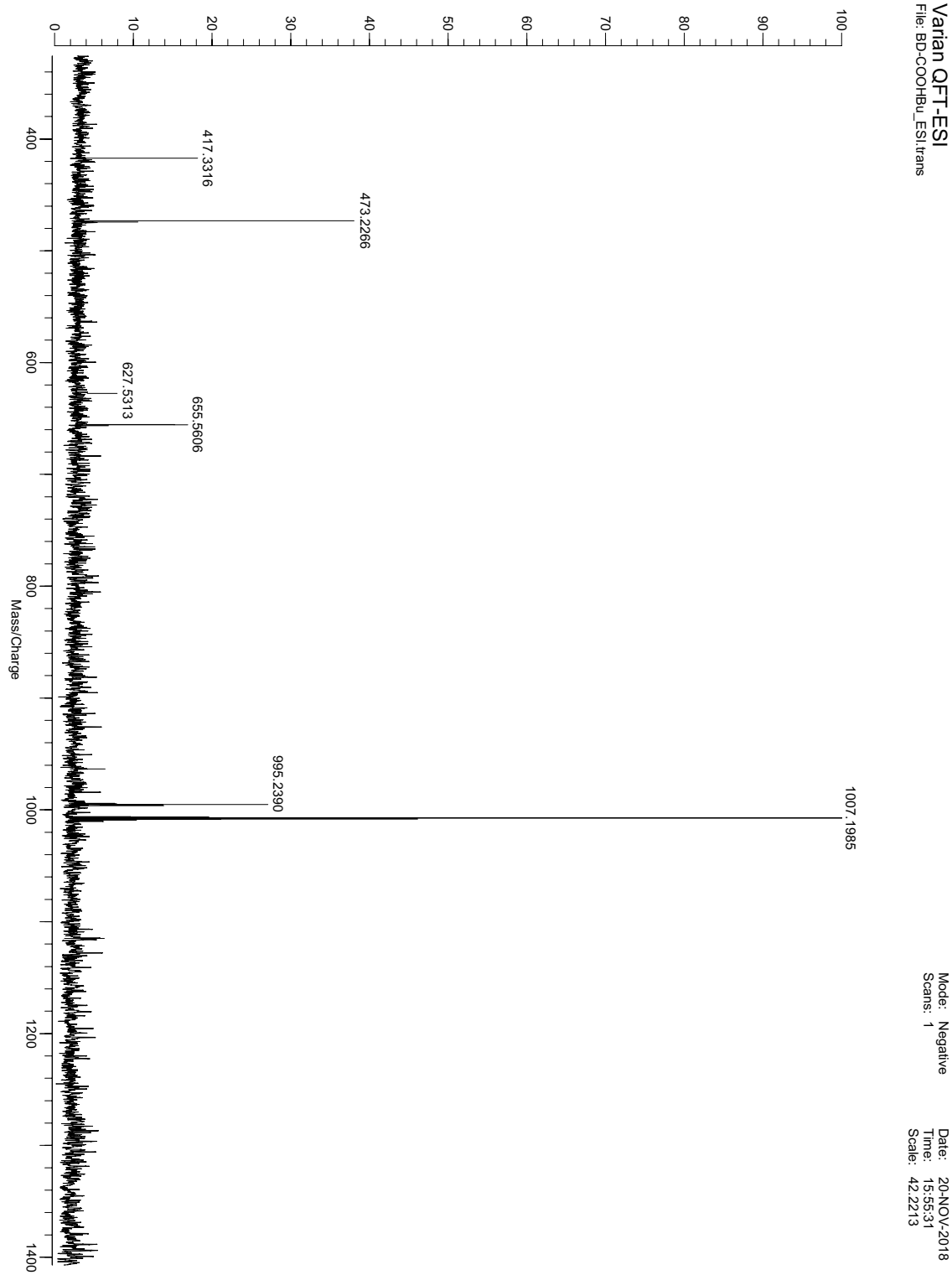

Figure S53. HRMS of **BD-COOH$_{Bu}$**.

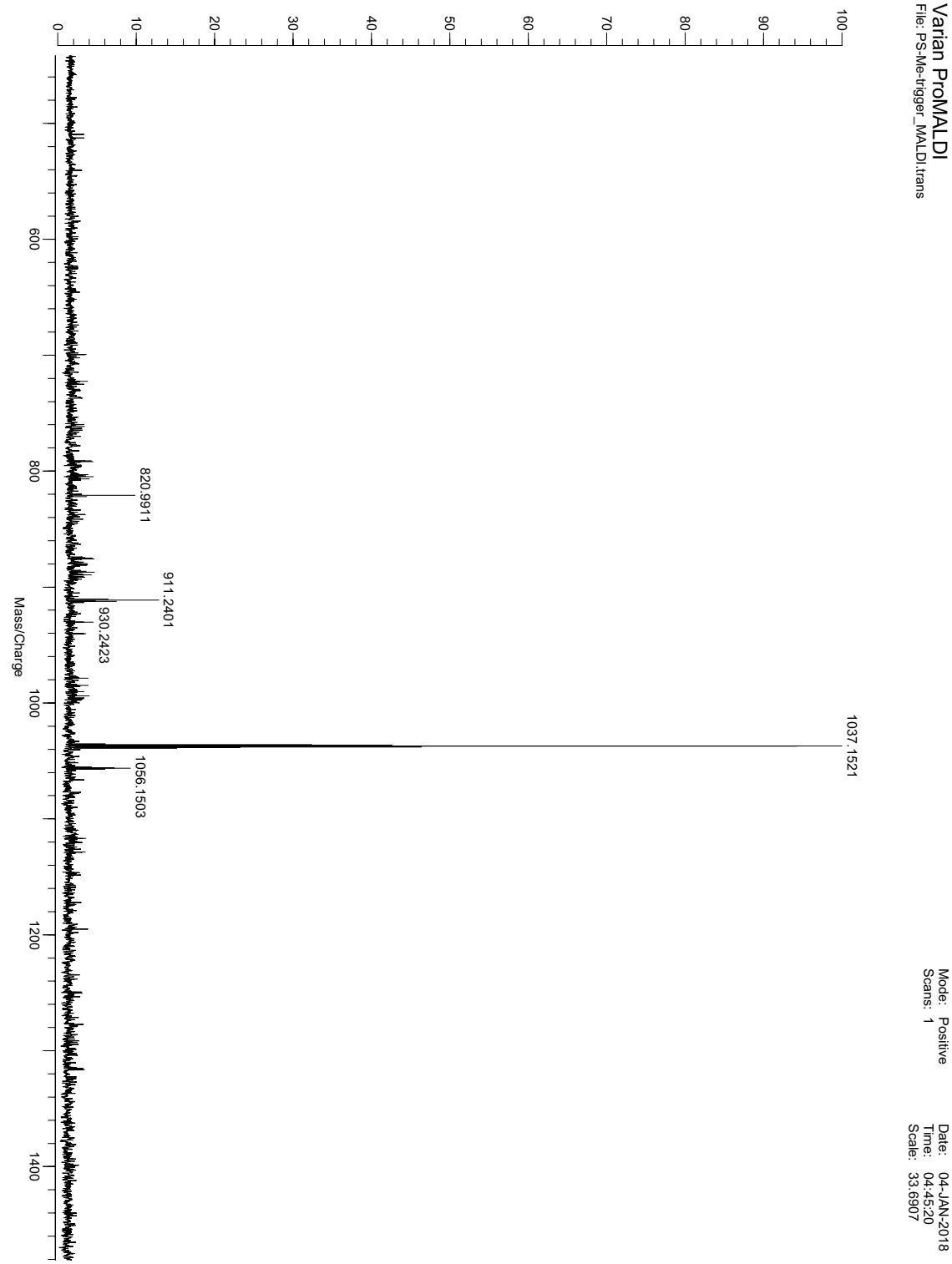

Figure S54. HRMS of **BD-PG$_{Me}$**.

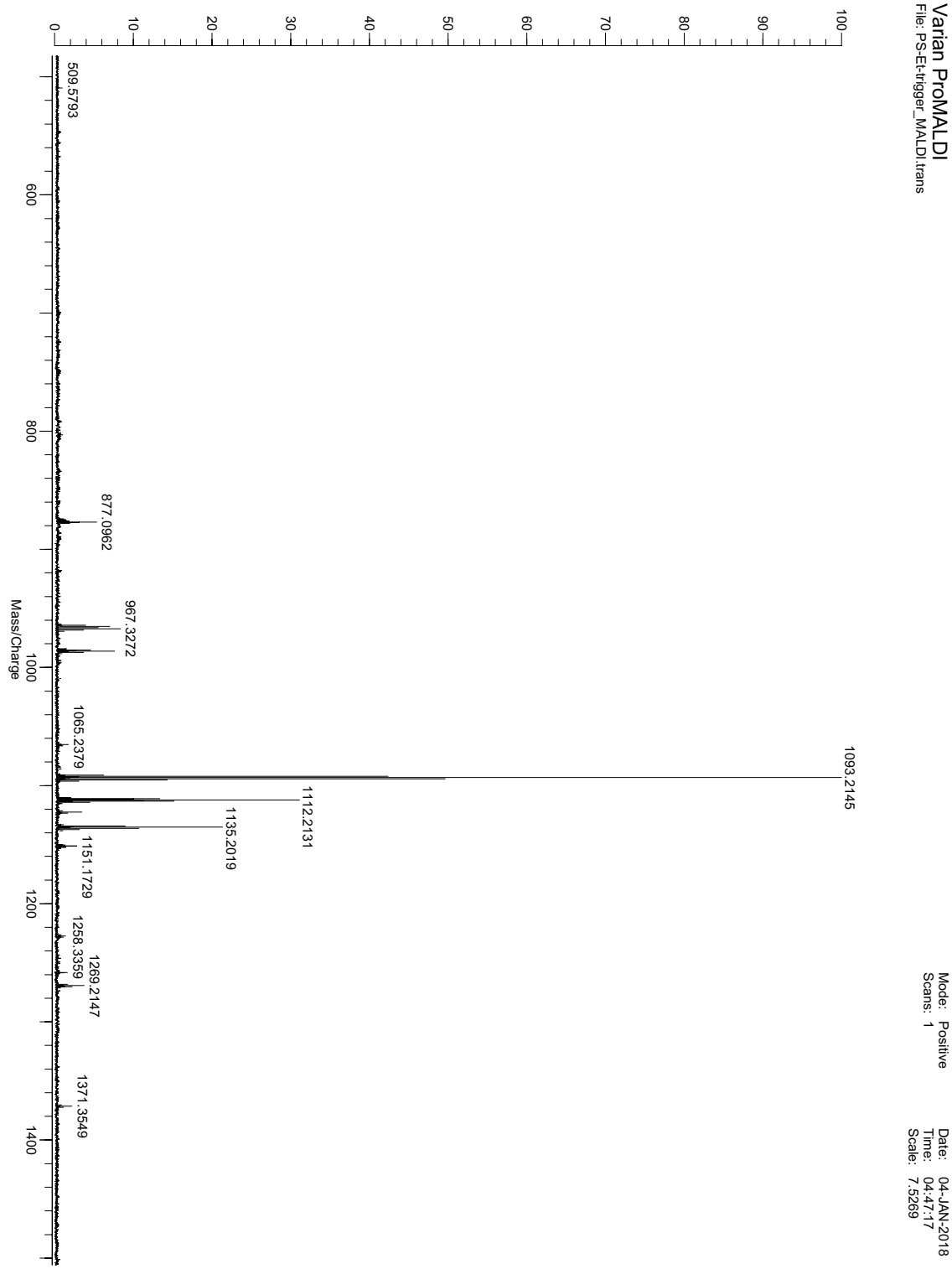

Figure S55. HRMS of **BD-PG$_{Et}$**.

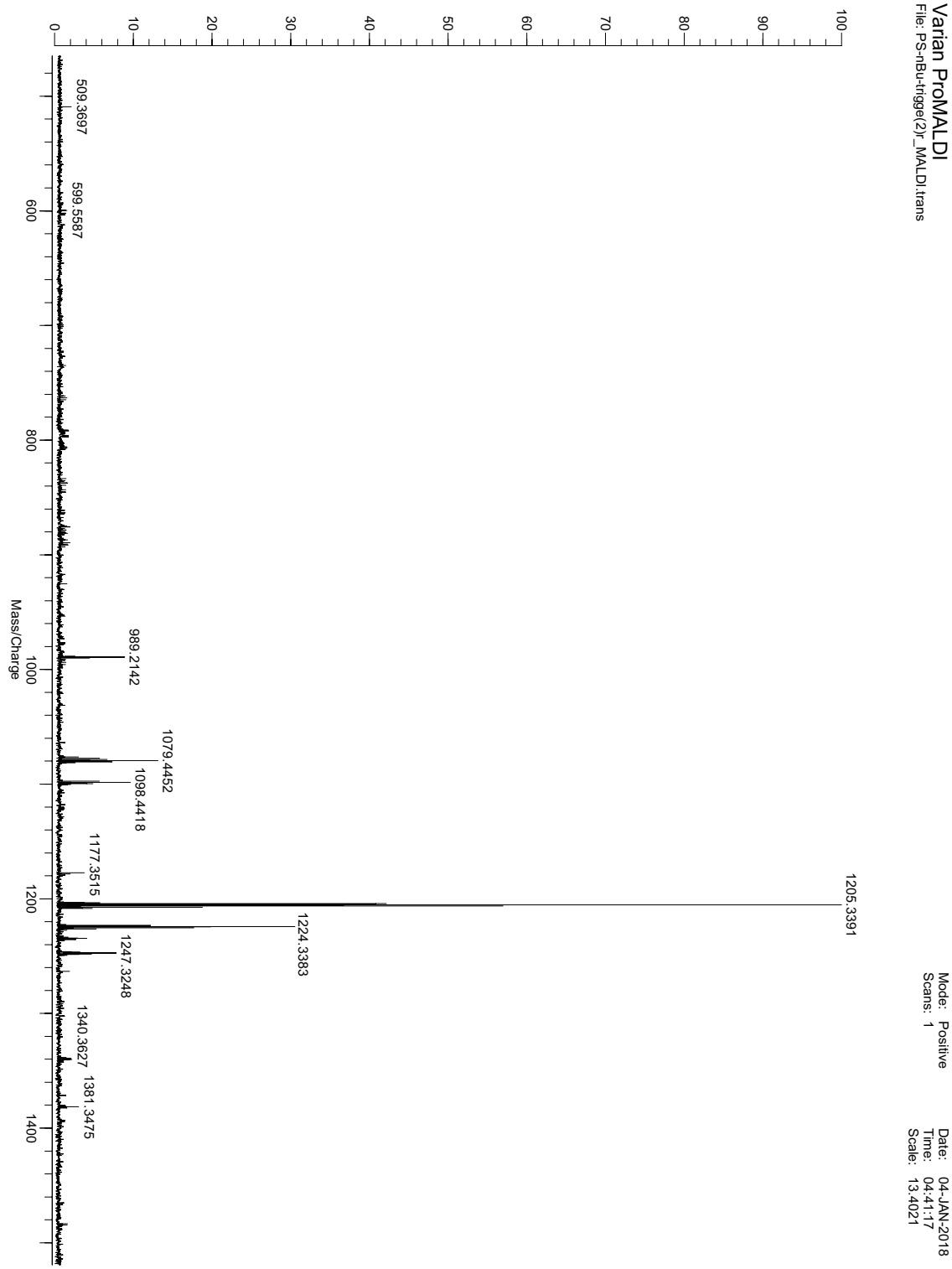

Figure S56. HRMS of **BD-PG$_{Bu}$**.

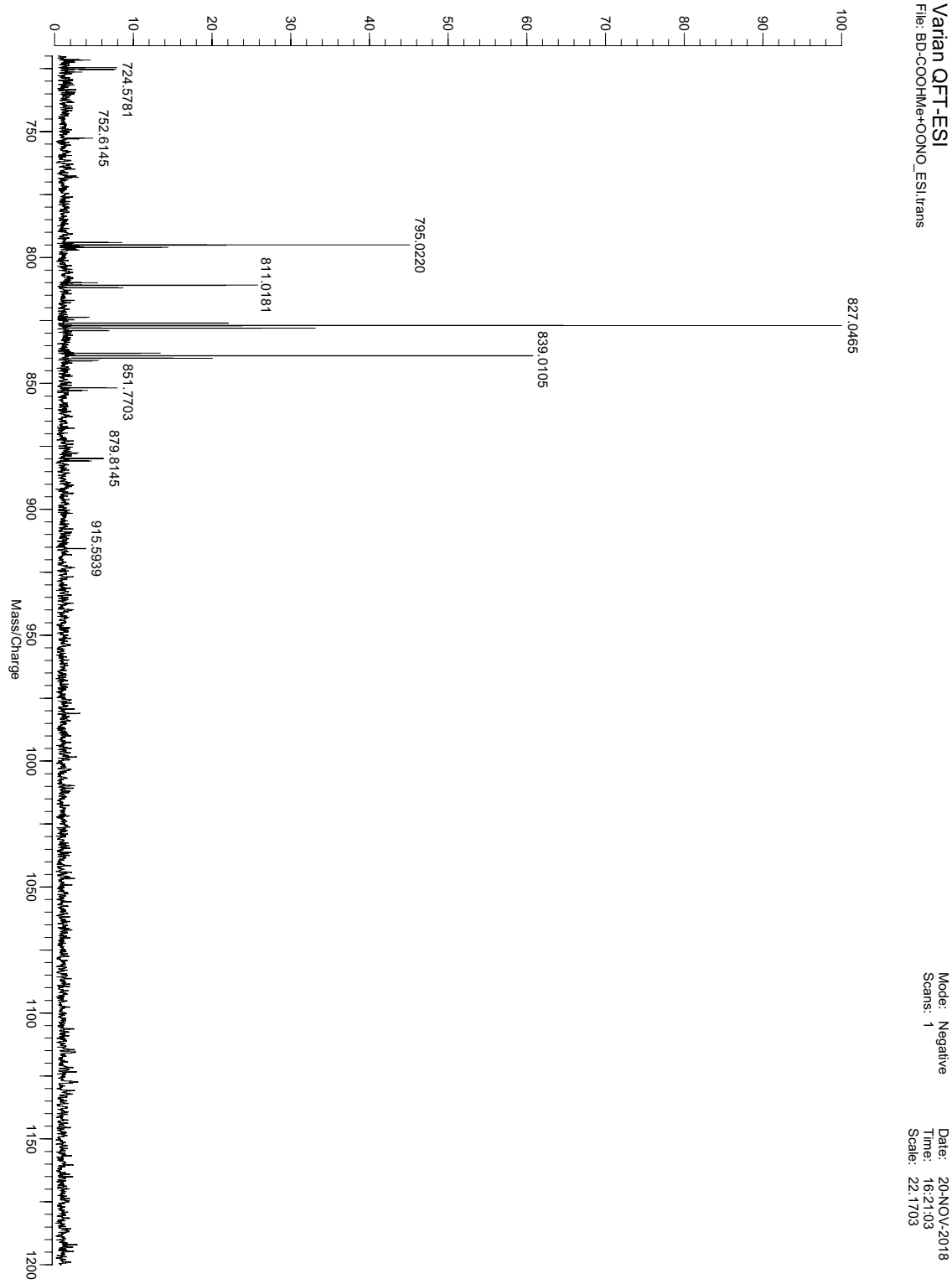

Figure S57. HRMS of the assay solution of **BD-PG$_{Me}$** after 30 min incubation with peroxynitrite.

8. References

(1) Armarego, W. L. F.; Perrin, D. D. *Purification of Laboratory Chemicals,* Butterworth-Heinemann, **2000.**

(2) Chen, H.; He, X.; Su, M.; Zhai, W.; Zhang, H.; Li, C. A General Strategy Toward Highly Fluorogenic Bioprobes Emitting across the Visible Spectrum. *J. Am. Chem. Soc.* **2017,** *139,* 10157-10163.

(3) Abrams, M. L.; Foarta, F.; Landis, C. R. Asymmetric Hydroformylation of Z-Enamides and Enol Esters with Rhodium-Bisdiazaphos Catalysts. *J. Am. Chem. Soc.* **2014,** *136,* 14583-14588.

(4) Charisiadis, A.; Bagaki, A.; Fresta, E.; Weber, K. T.; Charalambidis, G.; Stangel, C.; Hatzidimitriou, A. G.; Angaridis, P. A.; Coutsolelos, A.G.; Costa, R. D. Peripheral Substitution of Tetraphenyl Porphyrins: Fine-Tuning Sself-Assembly for Enhanced Electroluminescence. *ChemPlusChem* **2018,** *83,* 254-265.

(5) Amat-Guerri, F.; Lempe, E.; Lissi, E. A.; Rodriguez, F. J.; Trull, F. R. Water-Soluble 1,3-Diphenylisobenzofuran Derivatives Synthesis and Evaluation as Singlet Molecular Oxygen Acceptors for Biological Systems. *J. Photoch. Photobio.* **1996,** A *93,* 49-56.

(6) Wang, Y.; Tang, L.; Sun, T.; Li, C.; Xiong, M.; Wang, J. Self-Assembled Micelles of Biodegradable Triblock Copolymers Based on Poly(ethyl ethylene phosphate) and Poly(ε-caprolactone) as Drug Carriers. *Biomacromolecules* **2008,** *9,* 388-395.

(7) Chen, Z.; Liu, Y.; Wagner, W.; Stepanenko, V.; Ren, X.; Ogi, S.; Würthner, F. Near-IR Absorbing J-Aggregate of An Amphiphilic BF_2-Azadipyrromethene Dye by Kinetic Cooperative Self-Assembly. *Angew. Chem. Int. Ed.* **2017,** *56,* 5729-5733.

(8) Weingarten, A. S.; Kazantsev, R. V.; Palmer, L. C.; Mcclendon, M. T.; Koltonow, A. R.; Samuel, A. P. S.; Kiebala, D. J.; Wasielewski, M. R.; Stupp, S. I. Self-Assembling Hydrogel Scaffolds for Photocatalytic Hydrogen Production. *Nat. Chem.* **2014,** *6*, 964-970.

(9) Adarsh, N.; Avirah, R. R.; Ramaiah, D. Tuning Photosensitized Singlet Oxygen Generation Efficiency of Novel Aza-BODIPY Dyes. *Org. Lett.* **2010,** *12,* 5720-5723.

(10) Mirenda, M.; Strassert, C. A.; Dicelio, L. E.; San Roman, E. Dye-Polyelectrolyte Layer-By-Layer Self-Assembled Materials: Molecular Aaggregation, Structural Stability, and Singlet Oxygen Pphotogeneration. *ACS Appl. Mater. Interfaces.* **2010,** *2,* 1556-1560.

(11) Redmond, R. W.; Gamlin, J. N. A Compilation of Singlet Oxygen Yields from Biologically Relevant Molecules. *Photochem. Photobio.* **1999,** *70,* 391-475.

(12) Jung, H. S.; Han, J.; Shi, H.; Koo, S.; Singh, H.; Kim, H.; Sessler, J. L.; Lee, J. Y.; Kim, J. H.; Kim, J. S. Overcoming the Limits of Hypoxia in Photodynamic Therapy: A Carbonic Anhydrase IX-Targeted Approach. *J. Am. Chem. Soc.* **2017,** *139,* 7595-7602.

(13) Kim, H.; Kim, Y.; Kim, I. H.; Kim, K.; Choi, Y. ROS-Responsive Activatable Photosensitizing Agent for Imaging and Photodynamic Therapy of Activated Macrophages. *Theranostics* **2014,** *4,*1-11.

(14) Cheng, Y.; Cheng, H.; Jiang, C.; Qiu, X.; Wang, K.; Huan, W.; Yuan, A.; Wu, J.; Hu, Y. Perfluorocarbon Nanoparticles Enhance Reactive Oxygen Levels and Tumour Growth Inhibition in Photodynamic Therapy. *Nat. Commun.* **2015,** *6,* 8785.

(15) Idris, N. M.; Gnanasammhan, M. K.; Zhang, J.; Ho, P. C; Mahendran, R.; Zhang, Y. In Vivo Photodynamic Therapy Using Upconversion Nanoparticles as Remote-Controlled Nanotransducers. *Nat. Med.* **2012,** *18,* 1580-1585.